

EVALUATION OF THE BENDING PROPERTIES OF PROFILED SKIN STRUCTURE

Hassan Al Qaraghuli

A Thesis Presented to the Faculty of the
American University of Sharjah
College of Engineering
In Partial Fulfillment
Of the Requirements
For the Degree of

Master of Science in
Civil Engineering

Sharjah, United Arab Emirates

January 2016

Approval Signatures

We, the undersigned, approve the Master's Thesis of Hassan Al Qaraghuli.

Thesis Title: Evaluation of the bending properties of profiled skin structure

Signature

Date of Signature
(dd/mm/yyyy)

Dr. Adil K. Al-Tamimi
Professor, Department of Civil Engineering
Thesis Advisor

Dr. Monji Ben Ouezdou
Visiting Professor, Department of Civil Engineering
Project Committee Member

Dr. Tarik Ozkul
Professor, Dept. of Computer Science and Engineering
Project Committee Member

Dr. Aliosman Akan
Head, Department of Civil Engineering

Dr. Mohamed Guma El-Tarhuni
Associate Dean, College of Engineering

Dr. Leland Thomas Blank
Dean, College of Engineering

Dr. Khaled Assaleh
Interim Vice Provost for Research and Graduate Studies

Acknowledgements

I would like to express my gratitude to my project supervisors, committee members, family and friends, without whom the completion of this research would have never been possible. Words are not enough to express my feelings to people who helped me to reach what I have always been dreaming about. First and foremost, I would like to thank Dr. Adil Al-Tamimi, my thesis supervisor and Dr. Basim Abbas, the industrial advisor for their supervision, motivation and guidance throughout the research program and for believing in my ability to finish this project and guiding me through the right path to success. I am also grateful to Dr. Hayder Yasir for his supportive comments and encouragements. Moreover, I would like to thank the company Middle East Insulation “MEI” for funding this project. I would also like to acknowledge Eng. Arshi Faridi and Eng. Mohammad Ansari for their support during the experimental stage of this research and for supervising and controlling the experiment trials. Many thanks also go to my parents and my wife for their love and support. They truly helped me to see myself achieving my goals. Finally, I would like to acknowledge their honest feedback and encouragement to finish this research and during the entire Master’s program.

Dedication

This thesis is dedicated to my father, role model, and best friend Dakhel Hassan Al Qaraghuli, to my mother Kawkab Badar, my supervisor Adil Al-Tamimi and my wife Alaa Tamimi. This work would not have been completed without their sacrifice, encouragement, and limitless belief in me. Dad, Mom, and my beloved wife, I will be in your debt forever. May Allah bless you all.

Abstract

This research is focused on developing a representative testing method for structural skin panels. The profiled panels are widely used in many applications used in warehouses and factories. They are mainly used as roof or wall cladding to resist uniformly distributed loads mostly imposed by wind loads. Existing mechanical tests include the operation of wind tunnels to apply uniform load on corrugated large surfaces. These wind tunnels are expensive to build, requires a large space and are time consuming. The main objective of this research is to develop an easier and realistic testing method to test these panels and provide accurate mechanical properties, such as the stiffness rigidity of the panels. A total of 54 samples of skin panels divided into 18 sets were tested. Each set consists of 3 samples of nearly 1.0 x 2.0 m in size. Sets are divided into different metals, shapes of corrugations (profiles), and thicknesses. Two types of metals were tested; galvanized steel and aluminum profiled sheets. To verify the value obtained from the laboratory, a theoretical calculation based on EN1999-4:2007 standards is calculated and compared with the British standard. Finally, a finite element model was developed to correlate laboratory and calculated results. The difference between the actual tested samples and the empirical calculations for the galvanized steel profiles was (0.31%-6.4%). The aluminum profiled sheets showed the same pattern which was (0%-7%). Furthermore, modeling by ABACUS showed close differences above the tested values which supports the current results. The results confirm that the new set up produced conservative measurements compared to the empirical calculations.

Search Terms: Skin panels, galvanized steel, aluminum, stiffness rigidity, finite element.

Table of Contents

Abstract.....	6
List of Figures	9
List of Tables	12
List of Symbols	
Chapter 1: Introduction.....	17
1.1 History of Profiled Metal Sheets.....	19
1.2 Research Objectives.....	20
Chapter 2: Literature Review.....	22
2.1 Introduction	22
2.1.1 Structural failure and roof collapse.....	23
2.1.2 Wind failure.....	24
2.2 Metal Sheet Testing for Uniform Load.....	25
Chapter 3: Research Methodology.....	34
3.1 Characteristics of the Materials.....	34
Chapter 4: Theoretical calculation.....	39
4.1 Profiled Steel Sheet Calculation of the Moment Capacity.....	39
4.1.1 Limit state design.....	39
4.1.2 Loading.....	39
4.1.3 Ultimate limit state.....	40
4.1.4 Serviceability limit state.....	40
4.1.5 The mechanical properties of steel.....	41
4.1.5 Calculation of the effective section	42
4.1.6 Design for lateral loading.....	48

4.1.7 Bending moment calculations for steel profiles.....	49
4.2 Design of Aluminum Cold Form Sheets.....	50
4.2.1 Material properties.....	51
4.2.2 Design of aluminum profile sheets.....	53
4.3 Testing Method.....	59
4.4 Modeling by Finite Element Method.....	66
Chapter 5: Results and Discussion.....	71
Chapter 6: Conclusion	91
References.....	93
Appendix	97
Vita.....	103

List of Figures

Figure 1: Profiled metal sheets types.....	18
Figure 2: Wind load forces on buildings.....	24
Figure 3: Effects of the wind on the structure.....	24
Figure 4: Load cases and bending moment of the profiled sheets	27
Figure 5: Loading set-up for Michael & Bartlett experiment	27
Figure 6: Testing set-up airbags for Mahaarachchi and Mahendranin	29
Figure 7: Air-box set-up	30
Figure 8: Magnetic field setup	31
Figure 9: MEI setup for sandwich panel testing	32
Figure 10: MEI setup for sandwich panel testing	32
Figure 11: Stress strain curve.....	35
Figure 12: Stress/ strain diagrams	37
Figure 13: Nominal yield strength & nominal ultimate tensile strength.....	42
Figure 14: Effective width for a stiffened element	43
Figure 15: K factors for stiffened compression flanges	45
Figure 16: Calculation of effective widths allowing for corner radii	45
Figure 17: Effective cross section of an unstiffened trapezoidal profile in bending	46
Figure 18: K factors for unstiffened compression flanges	47
Figure 19: Stress distributions over effective portions of web	48
Figure 20: Alternative methods for determining the moment capacity when $y_c < y_t$	50
Figure 21: Notional widths of plane cross-section parts b_p allowing for corner radii	52
Figure 22: Initial effective cross-section area A_s for intermediate stiffeners in (a) flange and (b) web.....	55
Figure 23: Bending moment resistance as a function of the slenderness	57
Figure 24: Effective cross-section for resistance to bending moments.....	58
Figure 25: Measure e_c for determination of effective thickness	59
Figure 26: The Built testing setup.....	60

Figure 27: The adjustable legs	61
Figure 28: The laser sensor	61
Figure 29: The laser sensor location in the frame.....	62
Figure 30: the Cell Load and the piston.....	63
Figure 31: Hydraulic pump	63
Figure 32: Load cell.....	64
Figure 33: Load cell display device.....	64
Figure 34: The loading control panel.....	65
Figure 35: The loading setup.....	66
Figure 36: FE model.....	67
Figure 37: Geometry of 8-node shell element with six degrees of freedom.	68
Figure 38: Sweep action.....	68
Figure 39: Beam behavior in the model.....	69
Figure 40: a) Micrometer calipe, b) Coating thickness Meter.....	71
Figure 41: Steel sheet profiles of MEI.....	72
Figure 42: Local buckling in the profiled sheet	72
Figure 43: Local buckling	73
Figure 44: Calculating the Moment of inertia graph.....	76
Figure 45: Steel profiles averaged testing values for different profiles.....	78
Figure 46: Aluminum profiles averaged testing values for different profiles.....	78
Figure 47: Moment of inertia vs. thickness for (GI 38/200) profile with different thicknesses.....	84
Figure 48: Moment of inertia vs. thickness for different profile with different thicknesses.....	84
Figure 49: Moment of inertia vs. thickness for (AL 38/200) profile with different thicknesses.....	85
Figure 50: Moment of inertia capacity for different profiles with the same thickness (0.7 mm)	85
Figure 51: Moment of inertia capacity for different profiles with the same thickness (0.7 mm)	86
Figure 52: Moment comparison between steel profiles and aluminum profile with the same thickness	87
Figure 53: The FE model.....	88

Figure 54: Deflected FE model.....	89
Figure 55: Moment comparison	90
Figure 56: MI comparison for (38/200) steel profile with different thicknesses	90

List of Tables

Table 1: Load factors and combinations	41
Table 2: Normal maximum permissible deflection for profiled sheeting under uniform distributed loads	41
Table 3: Partial factors for ultimate limit	51
Table 4: Partial factors for serviceability limit	51
Table 5: Parameters λ_{lim} and α	53
Table 6: Buckling coefficient K_{σ} for cross-section parts in compression	54
Table 7: Reduction factor χ_d	56
Table 8: The plate diminutions in the FE model.	70
Table 9: Steel sheet profiles type and thicknesses.	74
Table 10: Aluminum sheet profiles type and thicknesses.	75
Table 11: Steel sheet profiles type and thicknesses and their tested moment.	77
Table 12: Aluminum sheet profiles type and thicknesses and their tested moment.....	79
Table 13: Steel sheet profiles type and thicknesses and their theoretical moment.	80
Table 14: Aluminum sheet profiles type and thicknesses and their theoretical moment.....	81
Table 15: Steel sheet profiles type and thicknesses and their tested & theoretical moment....	82
Table 16: Aluminum sheet profiles type and thicknesses and their tested & theoretical moment.	83
Table 17: (38/200) Profiled steel sheet load and moment for finite element Model.....	88

List of Symbols

A_r	Total stiffened area comprising the flange stiffener plus the two adjacent effective portions of the flange
$A_{r,ef}$	Effective area of a flange stiffener
$A_{sa,ef}, A_{sb,ef}$	Effective cross-sectional area of a web stiffener
B_f	Width of a flange for flange curling
b	Flat width of an element
b_c	Width subject to compression at ultimate limit state
b_d	Developed width of a stiffened element
b_{eff}	Effective width of a compression element
$b_{ef,1}$ to $b_{ef,n}$	Effective widths of parts 1 to n of web
$b_{ef,ser}$	Effective width at serviceability limit state
b_r	Width of a stiffener
b_t	Width subject to tension at ultimate limit state
$b_{t,ser}$	Width subject to tension at serviceability limit state
D_p	Overall depth of the profile
D_w	Sloping distance between the intersection points of a web and flanges
E	Modulus of elasticity of steel
f_a	Average stress in a flange
f_c	Applied compressive stress
$f_{c,1}$ to $f_{c,n}$	Applied compressive edge stress
f_{ser}	Compressive stress at serviceability limit state
$f_{1,ser}$ to $f_{n,ser}$	Compressive stress at serviceability limit state
f_t	Applied tensile stress
G	Shear modulus of steel

h	D_w/b
h_a	Vertical distance from edge of a web stiffener to the compression flange
I_{eff}	Effective second moment of area of a section
I_{min}	Minimum required second moment of area of an effective edge stiffener
I_r	Second moment of area of a flange stiffener, about its own centroid
$I_{\text{sa}}, I_{\text{sb}}$	Second moment of area of a web stiffener
I_{ser}	Effective second moment of area at serviceability limit state determined at mid-span
K	Relative local buckling coefficient for an element
K_t	Statistical correction factor
κ	Statistical factor
k_s	Reduction factor for the crushing strength of a stiffened web
$k_{\text{sa}}, k_{\text{sb}}$	Factors used to determine k
k_v	Shear buckling coefficient
L	Span of a member between centers of supports
L_b	Length of the buckling wave in a stiffener
M	Applied moment at a given point on a section
M_c	Moment capacity of a section
p_{cr}	Local buckling strength of an element
$p_{\text{eff,cr}}$	Effective value of critical buckling strength
$p_{\text{r,cr}}$	Elastic critical buckling strength of a flange stiffener
$p_{\text{s,cr}}$	Elastic critical buckling strength of a single longitudinal web stiffener
p_y	Design strength of steel

R_p	Relative section properties coefficient
R_s	Relative strength coefficient
R_t	Relative thickness coefficient
R_y	Relative yield strength coefficient
R	Inside bend radius
r_m	Mean bend radius
s	Standard deviation
h_w	Web height measured between system lines of flanges;
S_w	Slant height of web, measured between midpoints of corners;
t	Net thickness of steel material
t_{eff}	Effective thickness of a perforated element
t_{nom}	Nominal thickness assumed in design
U_s	Minimum ultimate tensile strength of steel
u	Maximum deflection of a flange towards the neutral axis due to flange curling
w	Intensity of load at serviceability limit state
Y_s	Minimum yield strength of steel
y	Distance from the flange to the neutral axis
y_c	Distance of the compression flange from the neutral axis
y_t	Distance of the tension flange from the neutral axis
α	Coefficient of linear thermal expansion or elastic critical strength factor
β	Reduction factor for stiffener effectiveness
ε	$(280/p_y) 0.5$ (with p_y in N/mm ²)
γ_f	Overall load factor
γ_l	Variability of loading factor

g_m	Material strength factor
g_p	Structural performance factor
δ	Deflection
η	Perry coefficient
$\lambda, \lambda_1, \lambda_{ser}$	Dimensionless quantities used in effective width calculations
θ	Angle between a web and a flange
ν	Poisson's ratio
φ	Angle between two plane elements;
ϕ	Slope of the web relative to the flanges.
χ_d	Reduction factor for distortional buckling (flexural buckling of stiffeners)

Chapter 1: Introduction

Structural skin elements, such as corrugated panels, are used within a building envelope as part of the roof, and wall structure. Corrugated panels are made from various materials such as steel, aluminum, copper, PVC and fiber reinforced polymers (FRP). The use of these panels has increased over the years as a result of their cost, lightweight, good bearing capacity and ease of transportation. The corrugated panels come in different thicknesses, sizes and shapes, depending on their respective use. In addition to this, their corrugation comes as half –rectangles, arcs, trapezoidal or other shapes (Figure 1).The panels can be made from cold rolled steel, aluminum, stainless steel or other metals and consists of linear corrugated patterns [1]. Essentially, the corrugations increased the bending strength of the respective sheet in the direction perpendicular to the corrugations but not necessarily parallel to them [2]. Moreover, these corrugations can increase the axial capacity of the profiled metal sheet, all those properties can be calculated using the British standards for cold form metals (BS 5950:1995). However, it is worthwhile to note that increasing the corrugation size or number will reduce the effective cover width of the sheet and this will lead to an increase in the cost.

Usually, the stronger direction of each sheet is manufactured longer. Cold-formed metal profiles are manufactured by rolling or bending thin sheets of metal to desired shapes allowing efficient and light profiles to be used where conventional hot-rolled profiles prove to be uneconomic. One of the main advantages of cold-formed metal profiles is the great flexibility of cross-sectional shapes to the manufacturing process allowing many desired cross-sections to be achieved. The cross-sectional shape is the key element in enhancing the strength of cold-formed metal profiles as it controls the three fundamental buckling modes: local, distortional (for open profiles) and global. Cold-formed profiled metal sheeting and decking are well-established construction products and manufacturers make strenuous efforts to keep these products competitive in terms of the carrying capacity for a given weight of material [3].

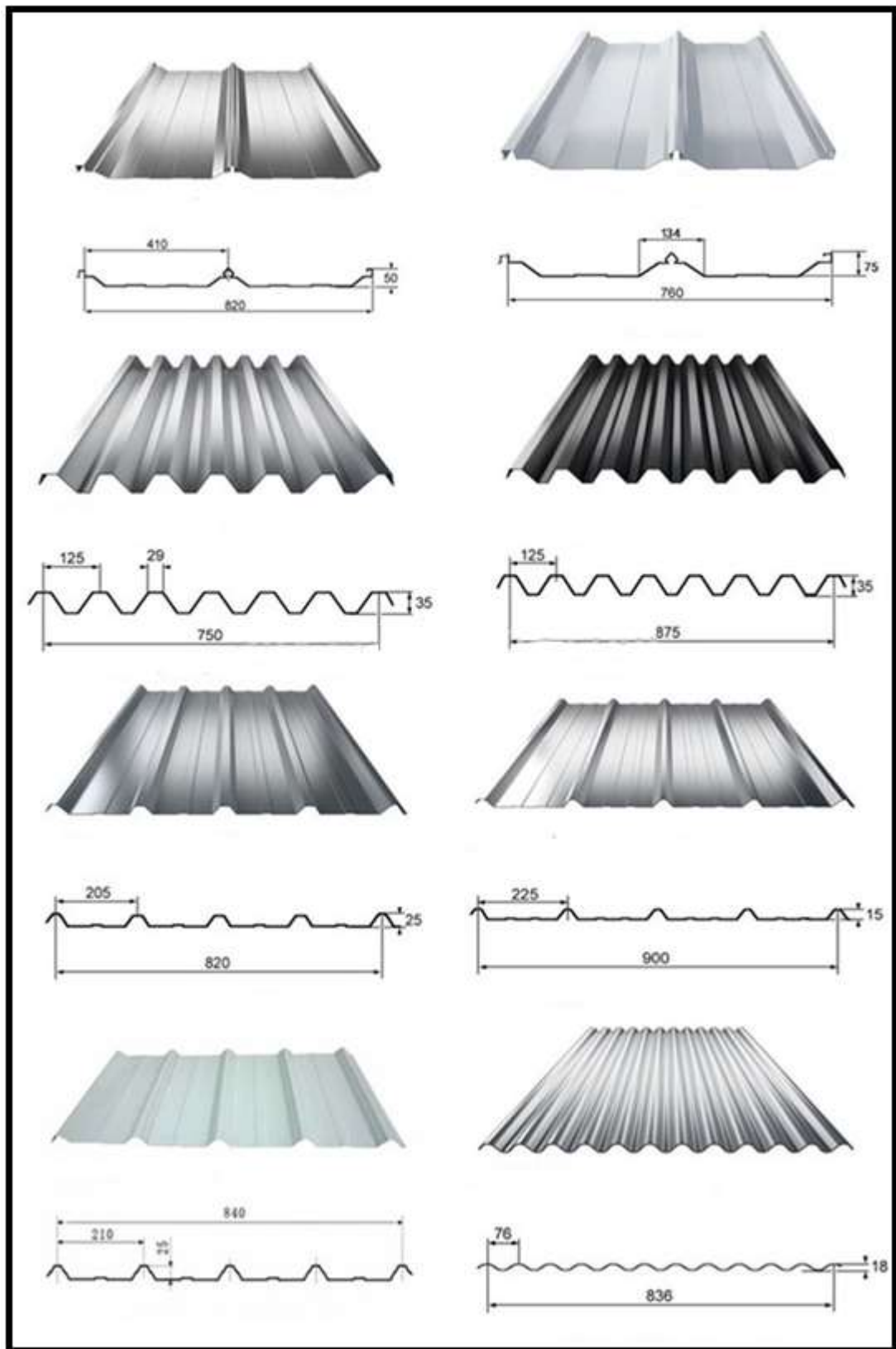


Figure 1: Profiled Metal Sheets Types [4]

Most sheeting and decking profiles can sustain considerable redistribution of bending moment so that the attainment of the calculated moment of resistance at an internal support is not immediately followed by failure. After yielding and/or buckling at the support, 'plastic hinge' action occurs, possibly accompanied by a reduction in the moment of resistance, until failure takes place when the full moment of resistance is attained within the span. Because, the mid-span moment of resistance is often greater than the reduced moment of resistance at the support, the increase in the load carried, as a result of this moment redistribute, can be considerable. Further plastic load resistance can be achieved through diaphragm action at the cost of excessive deflection [3].

Since the profiled metal sheets can be formed to many shapes to suit structural and constructional requirements, finding optimal shapes for cold-formed metal sections is a problem of great interest. The optimization of sections is aimed at achieving efficient use of the metal material either by maximizing the desirable properties of the section for a given mass and/or by minimizing the mass for a given application. Optimization of thin-walled metal sections is mostly performed to obtain improvements in strength, serviceability, and vibration characteristics [4].

The respective panels may come under three types of bending loads: point, line and uniform loads. Point loads occur from people walking on the panels whereas uniform loads occur as a result of wind or snow pressure or grain and liquids pressures in storage area. The issue with uniform loads is that it is difficult to simulate the load on the profiled sheets. Because of the many types of sheeting available and the diverse functional requirements and loading conditions the design and optimization of sheeting is generally based on experimental investigation [5].

1.1 History of Profiled Metal Sheets

Corrugated sheets were initially made from wrought iron and were introduced within the 1820's by Henry Palmer - an architect and engineer in the London Dock Company. The sheets evidently proved to be light, strong and transported relatively easily. It proved to be useful in terms of prefabricated structures. As a result, it was soon established as a common construction material in rural areas within the US, Chile, New Zealand, Australia and India. Later, it was also established as a frequent roofing material within urban areas. Moreover, in countries such as Australia and New

Zealand, it has become an integral part of the cultural identity in terms of fashionable architecture [2].

Profiled sheets are also a common construction material for industrial buildings around the world. The usage of the sheets has increased over the years for a number of reasons. This is because when it is compared to other materials, such as timber or concrete, the cold-form metal sheets possess the following advantages:

1. Lightness
2. High strength and stiffness to weight ratio
3. Ease of fabrication and mass production
4. Speed and ease of installation
5. Ease of transportation and handling

As a result of the above mentioned advantages, research had been conducted to determine its properties, as well as methods to improve it. A specific code is used to design the profile of a sheet which can provide the required strength [1].

The most sophisticated testing device that is available for testing metal roofs, other than the uniform static loading, has been the BRERWULF test setup. The test was initially developed by Cook, Keevil and Stobart [4], and the unsteady pressures produced in this test set-up remained spatially uniform. Clemson University used the test to re-create dynamic hurricane wind levels in the laboratory [5]. The tests were successful in terms of evaluating the boundary effects of the sheets under a hurricane simulation. On the other hand, this set-up did not provide the peak effective pressures that will be reached under the real hurricanes, because of that this set-up did not provide further insight with respect to the roof behavior before failure [5].

1.2 Research Objectives

- Develop a simple and practical testing set-up that simulates a uniform pressure over the profiled sheet.
- Measure and calculate the load and deflection of the sheets under the experimental loading.

- Calculate the mechanical properties of the sheets using British standard for Steel 5950-6:1995 and European Standards for Aluminum EN1999-4:2007code.
- Develop a finite element (FE) model for the profiled sheet under uniform pressure.
- Compare the experimental data and the theoretical and FE results.

Chapter 2: Literature Review

2.1 Introduction

The current standard design procedure, for that of wind loading, is based on statistical averages of wind tunnel data using weighted factors [2]. These factors are related to many elements such as the height, shape, location and terrain.

To reduce the complexity of pressure variations, the current British standard 5950-6:1995 design procedure specifies that metal buildings should be designed for uniform pressures over respective pressure zones: interior, edge, and corner [2]. The calculated static uniform reactions on the sheets in comparison to those that are caused by true wind loading remain questionable. The real wind does not apply a perfect uniform load on the sheets; it might be stronger in some places. However, in spite of the seriousness that is associated with the respective magnitude and steadiness of wind effects, uniform loads are still used for the design of the foundations that support the metal building, in addition to the framing, because structure designing factor of safety will reduce the impact of this issue [2]. Moreover, the corrugated sheets used for roofing and cladding are considered to be subject to bending moments which are caused by dead loads (the deadweight as well as the heat and damp insulations weight), live loads from maintenance or installation labors, and snow or wind. The loads are considered to be uniformly distributed.

In order for a structure to be sound and secure, the foundation, frame, walls, and roof must be strong and wind resistant. When building a structure, it is important to calculate the wind load to ensure that the structure can withstand high winds, especially if the building is located in an area known for inclement weather. Each wind load is determined by a probabilistic-statistical method based on the concept of “equivalent static wind load”, on the assumption that structural frames and components/cladding behave elastically in strong wind [6].

Usually, mean wind force (based on the mean wind speed) and fluctuating wind force based on a fluctuating flow field act on a building. The effect of fluctuating wind force on a building or part of a building depends not only on the characteristics of the fluctuating wind force but also on the size and vibration characteristics of the

building or part of a building. Low-rise buildings usually have low-pitched roofs and are subjected to uplift and racking loads during high-wind events. In addition to shear/racking forces in the sheeting, the wind action creates considerable pressures on both the upper surface and the underside of a roof/wall cladding. These forces may take the form of positive or negative pressure and must be considered in the design and fixing of a roof or wall. These recommendations evaluate the maximum loading effect on a building due to fluctuating wind force by a probabilistic-statistical method, and calculate the static wind load that gives the equivalent effect. The design wind load can be obtained from the summation of this equivalent static wind load and the mean wind load [6].

The wind force resisting system of a building is a vital component in the design of profiled skin sheets. However the wind load calculations can be difficult to figure out because the wind is unpredictable. Standard calculations can reveal good indication of what a building can withstand. Wind loading analysis is an essential part of the building process. If wind loading analysis is not done correctly the resulting effects could include collapsed windows and doors, ripped off roofing, and more [7].

Types of Wind Load Forces on Buildings:

- Shear Load – Wind pressure that is horizontal and could make a building tilt (Figure 2).
- Lateral Load – A pulling and pushing horizontal pressure that can cause a building to move off its foundation (Figure 2).
- Uplift Load – Pressures from wind flow that cause lifting effects (Figure 2).

2.1.1 Structural Failure and Roof Collapse

Although most roof-related failures are due to performance issues of the roofing system, there are a number of failure types that can be relatively more serious. These failure types can be strength related, and as a result, can cause significant damage within the roofing systems or even lead to a partial or full collapse of the respective building. The most relevant cause of these failure types is a direct result of overloading with respect to the roof elements. Regardless of whether the pressure is negative or positive,

if a roof is pushed past its limit, failure will result as a consequence. The most common type of strength related failure is wind uplift and overloading which are caused by excessive, snow, water and live load. The most critical one is the wind failure because of the uplifting effect which happens in the reverse side of the profile (the weak side) [8].

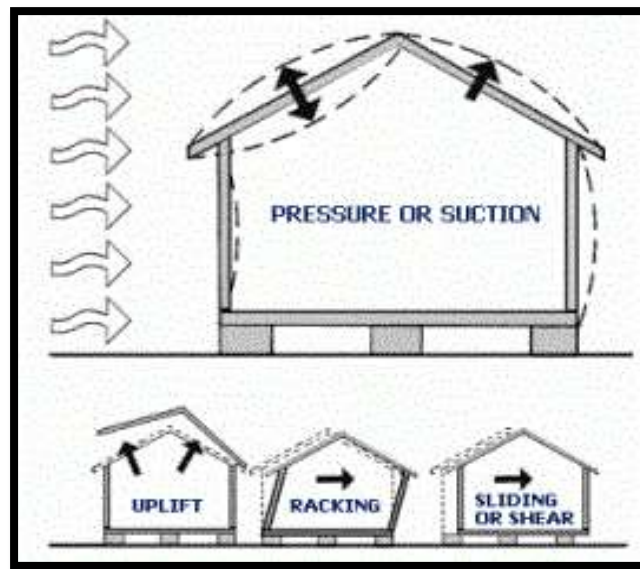


Figure 2: Wind Load Forces on Buildings [8]

2.1.2 Wind Failure

As wind interacts with a common roof structure, positive pressure will occur at the wind facing wall, while negative pressure will occur on the roof, as well as opposite and side walls (Figure 3). In a more realistic setting with a non-typical type roof, such as different roof elevations, the existence of large parapet walls, internal pressures - respective uplift forces can react differently. As a result, it is vital to analyze roof loads from one case to another or in other words, on a case to case basis.

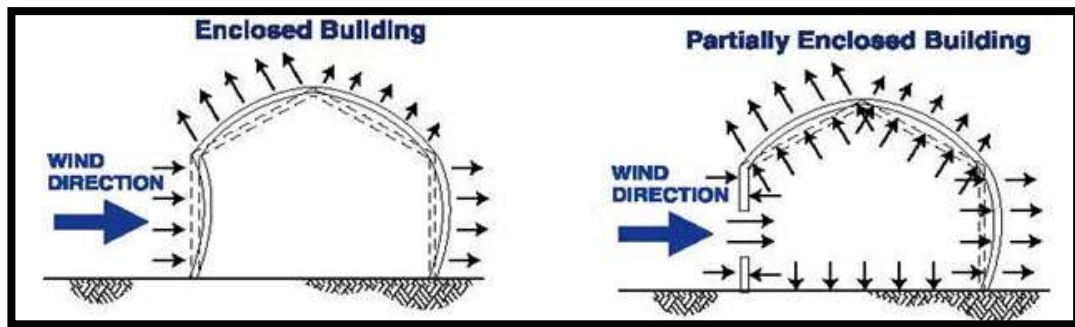


Figure 3: Wind pressure effects on the structure [9]

Wind uplift failures evidently occur when negative pressures of passing wind evidently pull up on the roof assembly of a structure. The uplift pressure causes stress-related damage to different roofing system parts, and as a result, exposes the interior or even facilitates failures in the structural assemble of the roof. This consequently causes partial or full roof collapse. The reason for this is that within a full size roofing situation, the main force resistance is taken by the sheets, as well as the attachment method to the deck. In situations where the sheets might be loose in between contact points, such as mechanically fastened bit, the profiled sheets can consequently be pulled by wind forces and this will cause the whole system to collapse [10]. The structure fails not only due to insufficient strength of the profiled sheets but also if the fasteners fail. It is absolutely vital to ensure fastener spacing along the perimeter of the system, as well as on the edge and corner substrate sections, thus meeting manufacturer guidelines and preventing uplift movement. Frequently, a testing standard instituted, such as Factory Mutual (FM) or Underwriters Laboratory (UL), will be used to rate the respective system that is being constructed. However, research shows that the overall result of positive pressure distortion with respect to a ribbed panel is essentially to increase the effective height of the rib, and as a result, increase both, the moment of inertia and consequently section modules. The shape will become stiffer and stronger. Furthermore, this increase of the load carrying capacity portrays a benefit in terms of more efficient use of materials.

With respect to uniform negative pressure, distortion will reduce both the moment of inertia, as well as section modules. In such a situation, panels with sloping ribs will appear to be more susceptible to change, as opposed to panels with narrow vertical ribs. Therefore, as the pressure increases, further distortion of the middle flat will induce a torsional force on the ribs which are evidently balanced by the adjacent panel and resisted by respective clip rigidity. Depending on the particular perimeter

attachment, the edge rib can actually be more or less resistant to rotation. Failure with respect to rib rotation and successive bulking may be more significant for those panels with symmetrical tall, narrow, vertical ribs, as opposed to trapezoidal ribs [11].

2.2 Metal Sheet Testing For Uniform Load

A large number of wind tunnel studies and field measurements have shown that roof and wall claddings in strong winds are subjected to wind suction or uplift forces [11]. Following Jensen's wind tunnel experiment, a number of full-scale and wind tunnel measurements simulated load on the low-rise buildings. These coefficients allow for the pressures on the small areas to be compared with the average increase over the surface. The uplift loading on the metal cladding is transferred to the battens or purlins below, then to the rafters or trusses and then to side wall or columns and finally to the foundation. Similarly the racking loads on the wall claddings are transferred to the wall studs, and the frame in the case of brick veneer walls, or girts in the case of metal cladding, then to the bracing walls or metal frames and finally to the foundation. This means there are two load paths. When transferring these load paths, there should not be any failure in a member or connection [12]. If either a member or connection in these paths is not capable of carrying the wind loading, the failure is initiated there and leads to a progressive collapse of the entire building. The severity of the failure depends on the weakest element in the structure and the type of connection. It is very important to design both members and connections with the same margin of safety. In other words, the roof should be secured to walls and walls to foundation, with all connections in place.

Furthermore, many researchers and institutes have tried to use other testing approaches to replace the wind tunnel method. The old method used dead weights and placing them on the panels. To act as a uniform load as J. D'Costa, Bartlett did in their testing. Point loads would be distributed using whiffle trees over the surfaces to approximate uniform pressures. Figure 4 shows that four equal point loads closely approximate the bending moments caused by a distributed load. The whiffle tree, as shown on Figures 4 and 5, is easily analyzed and relatively insensitive to deflections of the loaded surface [13]. To minimize cost, a means of applying the roof loads using water-filled 200 L drums was sought. Mechanical advantages were envisaged to affect

the total 10.4 kN roof uplift load from the 0.2 kN weight of the full drum, as shown schematically in Figure 4 and 5.

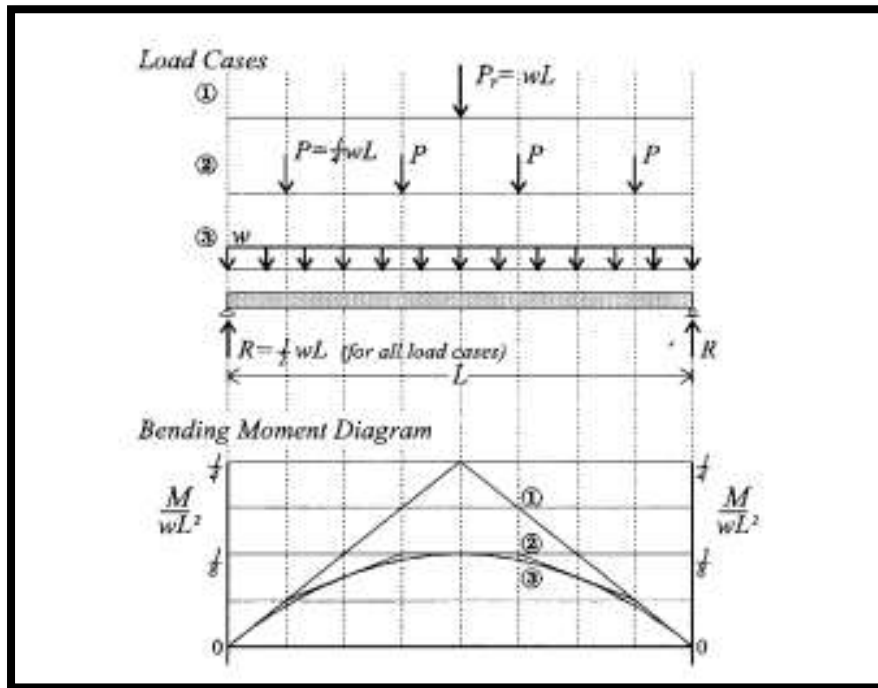


Figure 4: Load Cases and Bending Moment of the Profiled Sheets [14]

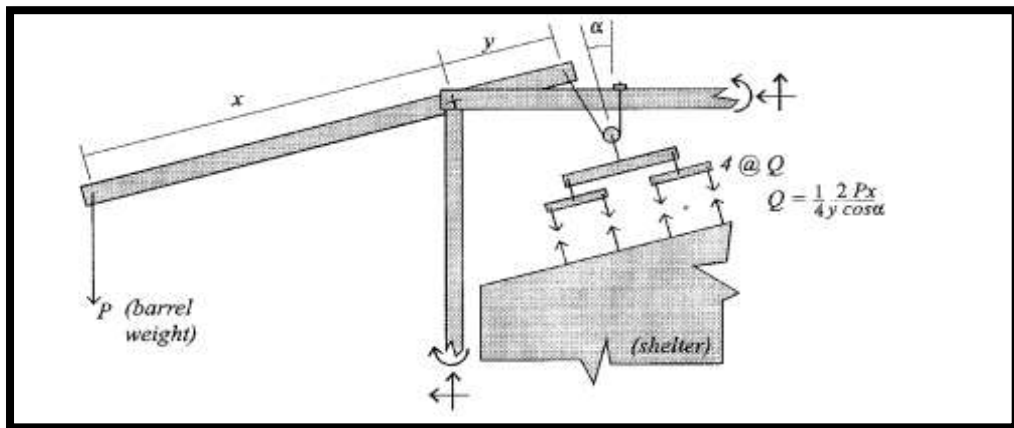


Figure 5: Loading set-up for Michael and Bartlett Experiment [14]

However, this method had many problems, including uneven distribution of load because of the size and shape of the individual weights, the inability to uniformly load a profiled shape, instability caused by deflection of the test specimen and uneven loading due to arching between the stacked elements. Of course, load cycling cannot be done this way. The more modern technique of using flexible plastic air bags that are inflated between the test specimen and a strong reaction frame overcomes most of

the problems associated with dead weights. Mahaarachchi and Mahendranin [15], analyzed and tested multi-span steel cladding assemblies. They used two-span steel cladding assembly with simply supported ends to model the critical regions of a multi-span cladding system under a uniform wind uplift pressure. Therefore, in their experiment, they tested the two-span cladding assembly with simply supported ends under a uniform wind uplift pressure loading in a rectangular air box of dimensions 1800 mm 4200 mm 300 mm (Figures 6 (a) and (b)). The test cladding assembly was set-up upside down inside the air-box, which was then sealed with 4.5 mm polythene sheets. The uniform wind uplift pressure was simulated by extracting the air from the air box using a vacuum pump. The gaps on both sides of the cladding assembly were filled with polystyrene foam. The results from this investigation including the design strength formulae can be used to evaluate safe and optimum loads for trapezoidal steel cladding with closely spaced ribs under wind uplift/suction forces. However, there is a potential shortcoming in the immediate vicinity of the sharp re-entrants in the profile of the test panel. While the airbag system may apply the correct total load to a surface, the airbag can arch across sudden profile changes and therefore may produce a different localized pressure distribution in the micro scale. In many circumstances this redistribution of local forces is minor and does not matter, but there may be cases where it could become critical.

Yet, the best approach was conducted by Henderson and Ginger [16]; they developed the “air-box” which solved most of the issues in the air bag system problems. The air-box is basically an open topped pressure chamber. It is 11 m long, 2 m wide and 0.5 m high as shown in Figure 7.

It is used to simulate wind pressure on structural elements, such as roof sheeting, wall cladding, structural panels, roof vents, skylights, windows, doors and other building elements. The air for the chamber is supplied under pressure by large twin fans. They can generate air pressure far in excess of what the strongest tropical cyclone would inflict on a house. This pressure can be made to simulate the positive pressure on the windward side, or the negative pressure (suction) on the lee side of a roof or building. Computer controlled valves in the system apply cyclic pressures to simulate the gustiness within a tropical cyclone or steady state pressure to simulate gale winds. The box can be divided into compartments so that strategic opening or closing of the inlet ducts can produce different pressures on adjacent spans of the test specimen.

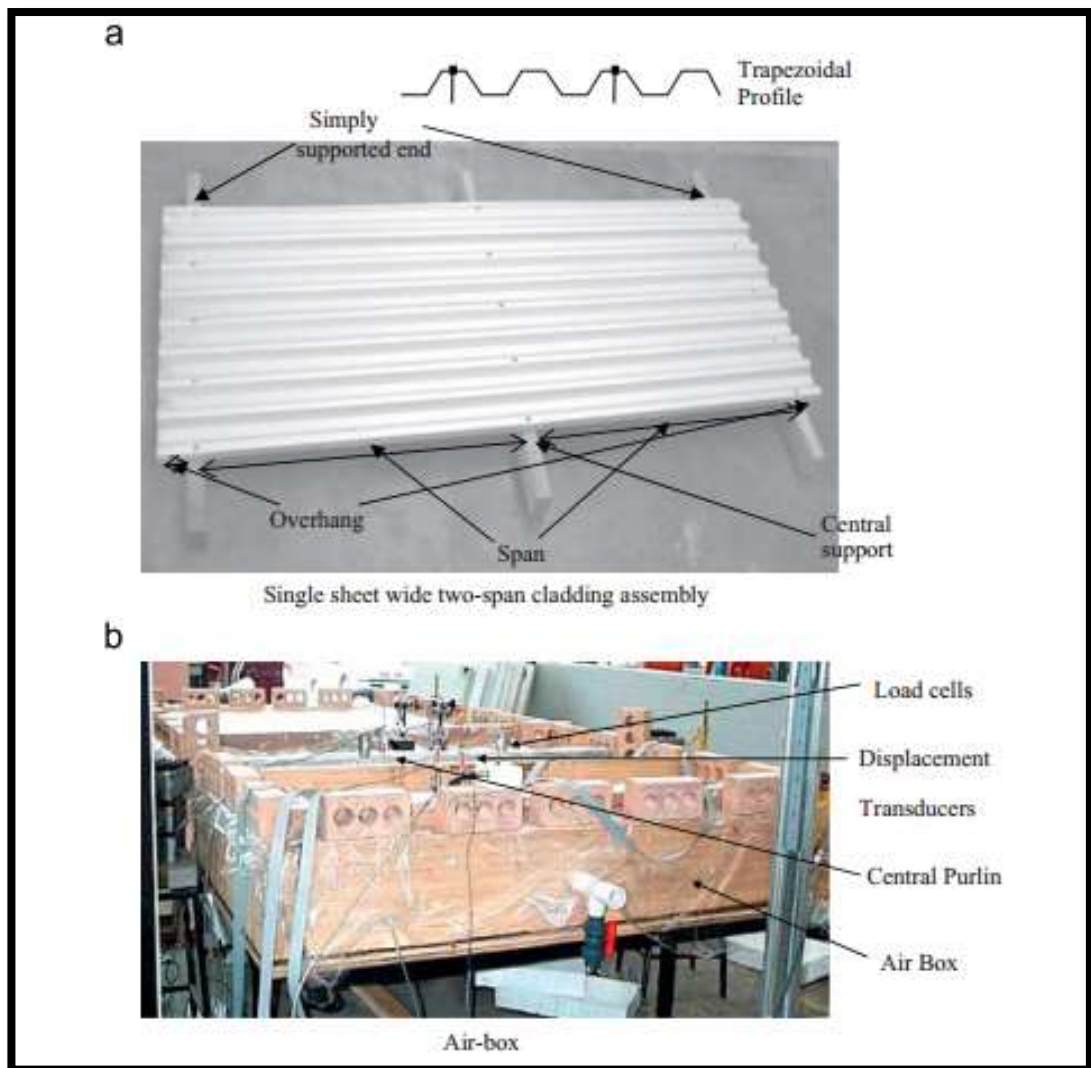


Figure 6: Testing Set-up Airbags for Mahaarachchi and Mahendranin [15]

Another attempt was constructed by Sinno [17] using the electromagnetic uplift loading test. This set up was based on the gap suspension of magnetic suction forces to apply in the simulating of wind tunnel loading on real full scale thin metal roofs. The applied simulated electromagnetic data was found to match the UWO wind tunnel data not only in time and space but also to duplicate the correlation coefficients of the wind tunnel data. Simulated loading for wind speeds from 50mph up to 160mph were applied and monitored at the rate of 20Hz (Figure 8).



Figure 7: Air-box set-up [16]



Figure 8: Magnetic Field Setup [17]

Additionally, a special setup was constructed by Abbas et al. [18] to test the flexural capacity of sandwich panels. Sandwich panels are a monolithic composite consisted of a top corrugated metal sheet made of thin steel or aluminum, low density rigid Polyurethane core, and a lower plain metal sheet. This setup is designed based on the flexure testing machine to perform the two point load test on the panels to measure the bending capacity of the profile. This setup has provided results that are matching with the British standards.

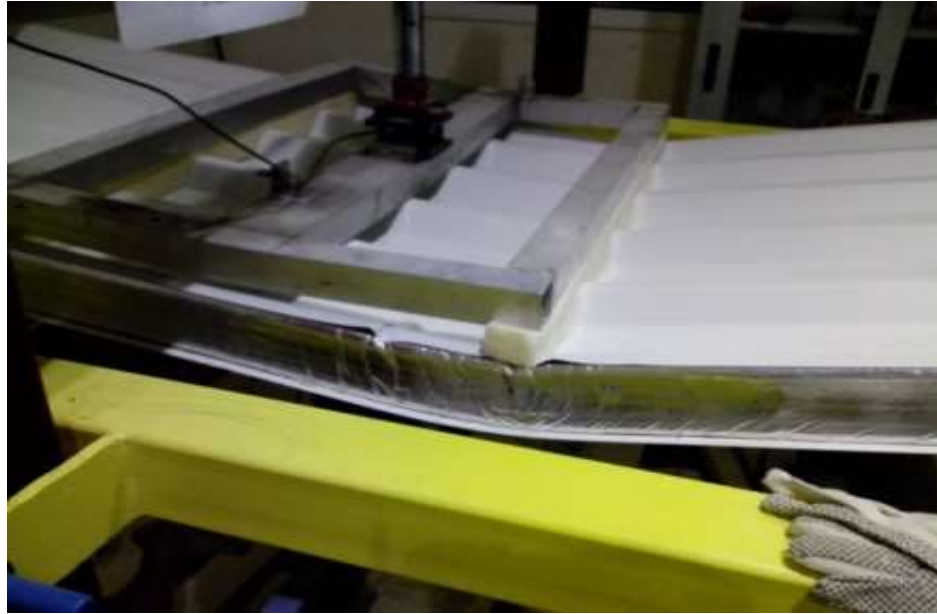


Figure 9: MEI Setup for Sandwich Panel Testing

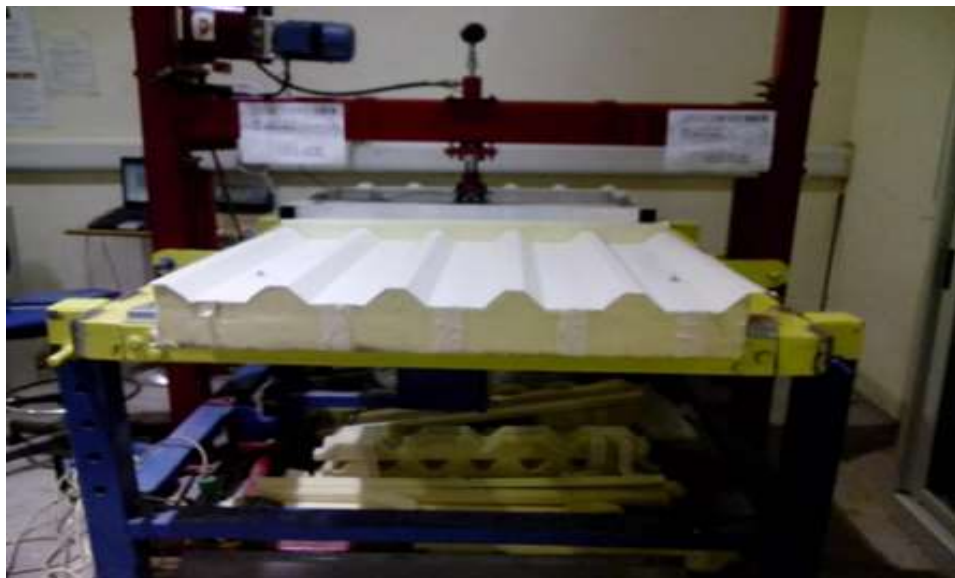


Figure 10: MEI Setup for Sandwich Panel Testing [18]

This study devised a purposely designed flexural machine suitable for laboratory tests with minimum cost. The machine is easy to operate and to set-up for different profile sheets testing under uniform load. The experimental part had to be coupled with theoretical calculations using existing mathematical equations to predict structural properties of the sheets. As a result of the easiness of the respective set up of the machine, time had been reduced as the tests had been conducted on the given site,

as opposed to sending the sheets across to the respective testing facility. Furthermore, by using the concept of a flexural machine, it was simpler to operate and consequently cost-effective. With the machine and loading set-up it can be an effective alternative to measure, verify, and predict the flexural behavior of the profile sheet used in many industrial buildings and shades.

Chapter 3: Research Methodology

The design process of corrugated sheet manufacturers includes tables specifying the limits of uniformly distributed loads within their product categories (for single, two and multi-span systems). Therefore this process involves extensive static-strength computations. These computations are essentially based on published equations which were developed from tests of certain profile elements. Many engineers prefer this design method for product design, as it is simple to evaluate variations of dimensions, thus arriving at an optimum shape. Furthermore, the procedure considers structure elements as strips or as parallel beams, and the flexural capacity is determined as a function of spacing elements and section properties.

On the other hand, single crosswise consideration made to determine the effective width of stability under compression loading. Iterative computations of the effective geometric as well as strength characteristics (effective cross sectional area A_{eff} , effective moment of inertia I_{eff} , effective section modulus W_{eff}) need to be determined in order to identify the deflections, (y), as well as the respective design resistances (moment MR , shear VR and bearing pressure FR), which is relatively time-consuming. The reason behind calculating the effective geometry is that the area of the profile gets reduced under the load to account for the local buckling that accrue in the profile.

3.1 Characteristics of the Materials

Generally, the grades of carbon steel and high strength low alloy steel, used for cold-formed steel products, are characterized by two main properties: the yield point and the tensile strength. Other important properties are ductility, hardness and weldability. The yield point of the steels commonly used for cold-forming ranges from 33 to 55 ksi (230 to 380 MPa), and may be higher. Tensile strength and ductility are important because of the way they relate to formability, and because of the local deformation demands of bolted and other types of connection. In members that include bolted connection or that, because of special design, may be subject to high stress concentrations, the tensile strength must be taken into account.

In the AISI Specification [1], fourteen different steels and aluminum are presently listed for the design of cold-formed steel members. Table 1 in the appendix lists steel designations, ASTM designations, yield points, tensile strengths, and

elongations for these steels. From a structural standpoint, the most important properties of steel are as follows:

1. Yield point or yield strength, F_y
2. Tensile strength, F_u
3. Stress-strain relationship
4. Modulus of elasticity, tangent modulus, and shear modulus
5. Ductility
6. Weldability

The panel has been tested for the yield strength and tensile strength to develop a stress-strain relationship curve, modulus of elasticity, tangent modulus, and shear modulus as shown below.

➤ **Modulus of Elasticity:**

$$E = \frac{\text{tensile stress}}{\text{extensional strain}} = \frac{\sigma}{\varepsilon} = \frac{F/A_0}{\Delta L/L_0} \quad (1)$$

where:

E is the Young's modulus (modulus of elasticity) (Figure 11)

F is the force exerted on an object under tension;

A_0 is the original cross-sectional area through which the force is applied;

ΔL is the amount by which the length of the object changes;

L_0 is the original length of the object.

➤ **Tangent modulus:**

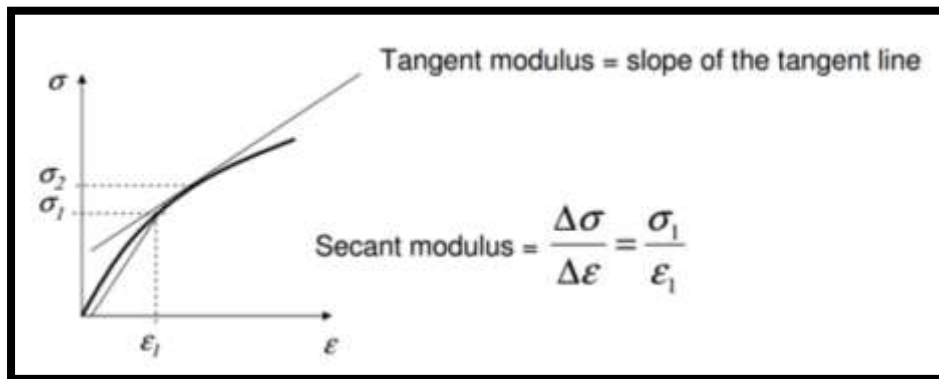


Figure 11: Stress Strain Curve

➤ Yield Point, Tensile Strength, and Stress-Strain Relationship

As listed in the Appendix, the yield points or yield strengths of all 14 different steels range from 33 to 55 ksi (230 to 380 MPa). The tensile strengths of the same steels range from 42 to 100 ksi (290 to 690 MPa). The ratios of the tensile strength-to-yield point vary from 1.12 to 2.22. As far as the stress-strain relationship is concerned, the stress-strain curve can either be the sharp-yielding type (Figure 12a) or the gradual-yielding type (Figure 12b).

➤ Strength Increase from Cold Forming

The mechanical properties (yield point, tensile strength, and ductility) of cold-formed steel sections, particularly at the corners, are sometimes substantially different from those of the flat steel sheet, strip, plate, or bar before forming. This is because the cold-forming operation increases the yield point and tensile strength and at the same time decreases the ductility. The effects of cold-work on the mechanical properties of corners usually depend on several parameters. The ratios of tensile strength-to-yield point, $(\frac{F_u}{F_y})$, and inside bend radius-to-thickness, r/t , are considered to be the most important factors to affect the change in mechanical properties of cold-formed steel sections. Design equations are given in the AISI-1996 Specification [1] for computing the tensile yield strength of corners and the average full-section tensile yield strength for design purposes.

➤ Modulus of Elasticity, Tangent Modulus, and Shear Modulus

The strength of cold-formed steel members that are governed by buckling depends not only on the yield point but also on the modulus of elasticity, E , and the tangent modulus E_t . A value of $E = 29,500$ ksi (203 GPa) is used in the AISI-1996 Specification [1] for the design of cold-formed steel structural members. The modulus of elasticity is slightly larger than the value of 29,000 ksi (200 GPa), which is being used in the AISC Specification for the design of hot-rolled shapes. The tangent modulus is defined by the slope of the stress-strain curve at any given stress level as shown in Figure 12b. For sharp-yielding steels, $E_t = E$ up to the yield, but with gradual-yielding steels, $E_t = E$ only up to the proportional limit, f_{pr} (Figure 12b). Once the stress exceeds the proportional limit, the tangent modulus E_t becomes progressively smaller than the initial modulus of elasticity. For cold-formed steel

design, the shear modulus is taken as $G = 11,300$ ksi (77.9 GPa) according to the AISI Specification [1].

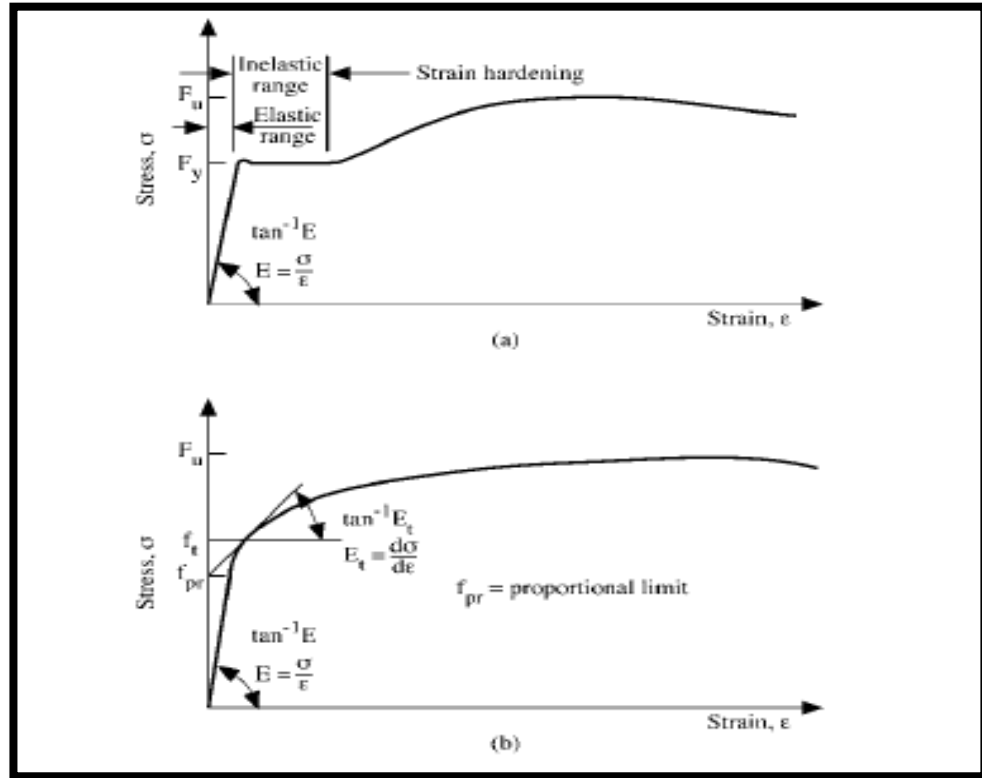


Figure 12: Stress/ Strain Diagrams [1]

➤ Ductility

The materials selected for the external envelop of a building can have a significant effect on its durability and the amount of maintenance that will be necessary during its life. The components that are exposed to the weather are particularly important. The type of sheeting material, coating and color must all be considered. The performance might also depend on the shape and orientation of the building and the environment. Generally, light colored coatings are preferable because they do not absorb as much sunlight as dark colors, and they are therefore cooler. This means they tend to have the best life and they optimize the thermal performance of an exposed roof [8]. According to the AISI specification [1], the ratio of $F_u = F_y$ for the steels used for structural framing members should not be less than 1.08, and the total elongation should not be less than 10% for a 2-in. (50.8 mm) gage length. If these requirements cannot be met, an exception can be made for purlins and girts, for which the following limitations should be satisfied when such a material is used: (1) local elongation in a 1/2-in. (12.7 mm) gage

length across the fracture should not be less than 20% and (2) uniform elongation outside the fracture should not be less than 3%. It should be noted that the required ductility for cold-formed steel structural members depends mainly on the type of application and the suitability of the material. The same amount of ductility that is considered necessary for individual framing members may not be needed for roof panels, siding, and similar applications. For this reason, even though structural grade 80 of ASTM A653 steel, grade *E* of A611 steel, and grade 80 of A792 steel do not meet the AISI requirements of the $F_u = F_y$ ratio and the elongation, these steels can be used for roofing, siding, and similar applications provided that (1) the yield strength, F_y , used for design is taken as 75% of the specified minimum yield point or 60 ksi (414 MPa), whichever is less, and (2) the tensile strength, F_u , used for design is taken as 75% of the specified minimum tensile stress or 62 ksi (427 MPa), whichever is less.

Chapter 4: Theoretical Calculations

4.1 Profiled Steel Sheet Calculation of the Moment Capacity

Designing of profiled sheets differs from one material to other. In this study, the focus will be on two type of metals, steel and aluminum. Both of those metals have different properties that will affect the strength of the profiled sheet.

4.1.1 Limit State Design Of Steel Sheet

Profiled steel sheeting should be designed by applying suitable factors for the ultimate limit state and the serviceability limit state, taking into consideration it would not reach a limit state at which it would become unfit for its intended use. The overall factor in any design has to cover variability of:

- Material strength
- Loading
- Structural performance
- Calculation accuracy
- Geometrical deviations

4.1.2 Loading

All applied loads should be considered separately and any realistic combinations that will give the most critical effects on the element concerned should be considered. Loading conditions during erection should be consider in the design. There are five types of loads that are applied in the design of the profiled sheets, those loads are dead, imposed, temperature loads, earthquake loads and wind loading. The combination of these loads and the limiting factors are different depending on their intended use.

- Dead loads: Those loads come from the self-weight of the profiled sheet and they have factors that are specified in Table 1.
- Minimum imposed roof loads: In most cases those sheets are used as a cover for the structure. The imposed loads on roofs are either for decoration or

maintenance those loads are either with access or without access. Where there is regular traffic for the maintenance of services and other elements of the building, the choice between the two alternative loading intensities given in (BS 6399 : Part 3)[19] should be carefully considered.

- Equivalent line loads: These loads can be found in (BS 6399 : Part 3), should be considered as equivalent to line loads of 1.5 kN/m and 3 kN/m, respectively, in a direction transverse to the span of the sheeting. In multi-span arrangements, the number and location of the line loads should be that combination which produces the greatest bending moment in the sheeting, subject to being no more than one line load per span.
- Construction loads: it will occur on roof decking or roof cladding during construction of the system. Roofs with no access that are being designed for the minimum imposed roof loads - the equivalent line load of (1.5 kN/m) should be increased to 2 kN/m.
- Local roof loads: Profiled sheets used as roof decking or roof cladding should also be capable of supporting the local un-factored load, as defined in (BS 5427)
- Wind load: This is considered to be the biggest load on the system. It is created by the speed of the wind, it different from one place to other and it fluctuate depending on the time of the year and the height of the structure. Calculating wind loads are described in (BS 3699 Part 2) [19].

4.1.3 Ultimate Limit State

When designing the profiled sheet for the desired system, the applied load that is considered in the system should be factored in such a combination that will give the most critical case.

The load capacity of each sheet and its connections, as determined by the relevant provisions of this Part of BS 5950 [19], should be such that the factored loads would not cause failure.

4.1.4 Serviceability Limit State

Serviceability load combination is the summation of all the loads without factoring. Only 80% of the wind and imposed load are consider in the load

combination. Moreover, the construction load is not considered in the load combination. Deflection is the limit that measures the serviceability limit. An element should not exceed a limit that can cause a failure to its element or its connections. Those limits are specified in Table 2.

Table 1: Load Factors and Combinations [19]

Loading	Loading Factor Y_f
Dead load	1.4
Dead load restraining uplift or overturning	1.0
Dead load acting with wind and imposed loads combined	1.2
Imposed load	1.6
Imposed load acting with wind load	1.2
Wind load	1.4
Wind load acting with imposed load	1.2
Forces due to temperature effects	1.2
<i>NOTE 1. Dead loads may be taken as zero for wall cladding</i>	
<i>NOTE 2. Construction loads are treated as imposed loads</i>	

Table 2: Normal Maximum Permissible Deflection for Profiled Sheetting under Distributed Loads [19]

Load condition	Permissible deflection as a multiple of span	
	Roof cladding	Wall cladding
Dead	L/500	--
Dead and imposed	L/200	--
Dead and wind	L/90	L/120
<i>*Excluding roof-lights</i>		

4.1.5 The Mechanical Properties of Steel

The design strength P_y should be taken as Y_s but not greater than $0.84U_s$ where:

Y_s : Is the nominal yield strength (i.e. the higher yield strength, R_{eff} , or in the case of material with no clearly defined yield, either the 0.2 % proof stress, $R_{p,0.2}$, or the stress at 0.5 % total elongation, $R_{t,0.5}$ as specified in the relevant material standard);

U_s : Is the nominal ultimate tensile strength (i.e. the minimum tensile strength, R_m as specified in the relevant material standard);

- Modulus of elasticity $E = 205 \text{ kN/mm}^2$
- Shear modulus $G = E/2.6$ (i.e. $G = 79 \text{ kN/mm}^2$ approx.)
- Poisson's ratio $n = 0.30$
- Coefficient of linear thermal expansion $\alpha = 1231026/8C^\circ$

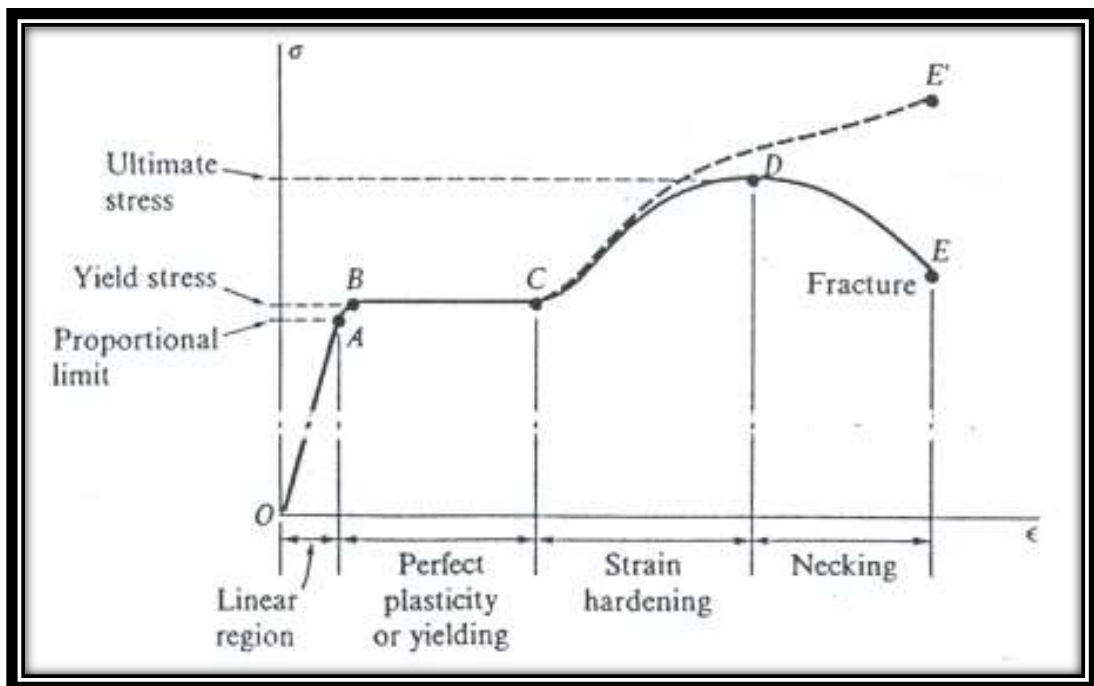


Figure 13: Nominal Yield Strength & Nominal Ultimate Tensile Strength [19]

4.1.5 Calculation of the Effective Section

When any part of the thin section is subjected to compressive force, local and global buckling are important factors that need to be considered during section properties calculation.

- **Local buckling:** Local buckling reduces the moment capacity and stiffness the profiled steel sheet. The amount of reduction can be calculated through the use of effective cross-sectional properties. These properties should be determined using:

- a) The effective widths of individual flat elements entirely or partially in compression.
- b) The effective areas of intermediate stiffeners for flat stiffened elements, the effective width consists of two portions, one adjacent to each edge (Figure 10).

For flat un-stiffened elements, all the effective width is located adjacent to the supported edge.

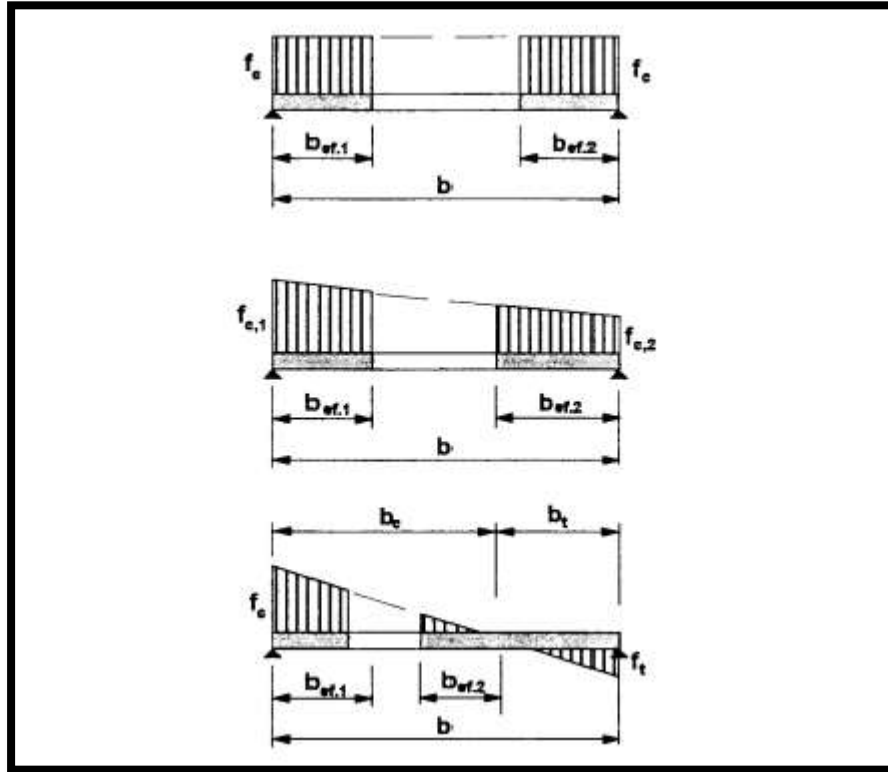


Figure 14: Effective Width for a Stiffened Element [19]

- **Effective width for strength calculations:** The ratio of the effective width b_{eff} to the flat width b of an element in compression should be determined from the following equations depending on the actual stress level available in the element.

- a) For $f_c/p_{cr} \leq 0.123$:

$$b_{eff}/b = 1$$

- b) For $f_c/p_{cr} > 0.123$:

$$\frac{b_{eff}}{b} = 1 + 14 \left(\left(\sqrt{\frac{f_c}{p_{cr}}} - 0.35 \right)^4 \right)^{-0.2} \quad (2)$$

where:

f_c is the applied compressive stress in the effective element.

p_{cr} is the local buckling strength of the element.

The local buckling strength p_{cr} (N/mm²) of an element can be determined from

$$p_{cr} = 0.904EK \left(\frac{t}{b}\right)^2$$

where:

K = is the relevant local buckling coefficient;

t = is the net thickness of the steel material;

b = is the flat width of the element.

The local buckling coefficient K depends upon the type of element and the geometry of the profile. For flanges stiffened at both longitudinal edges, the value of the buckling coefficient K may conservatively be taken as (4).

Alternatively a more precise value of K can be obtain from Figure 15 or determined from:

$$K = 7 - \left(\left(\frac{1.8}{0.15+h} \right) - \left(\frac{0.091}{h^3} \right) \right) \quad (3)$$

where:

$$h = \frac{D_w}{b};$$

D_w is the sloping distance between the intersection points of a web and the flanges.

b Is the flat width of the flange.

- **Effect of bend radius:** The effective width of a flat element should generally be calculated on the assumption that each element extends to the mid-point of the corners. When the inside bend radius r of a corner exceeds $5t$, the effective

width of each of the flat elements meeting at that corner should be reduced by $r_m \sin(\theta/2)$ (Figure 16).

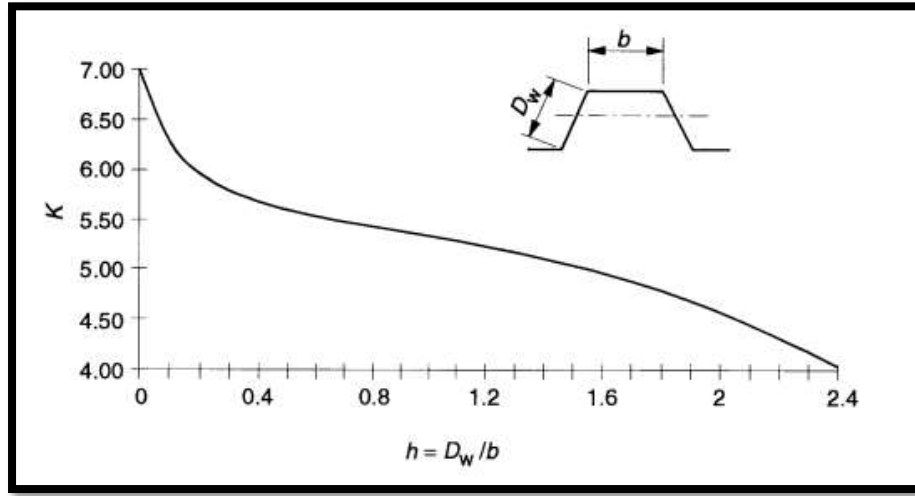


Figure 15: K Factors for Stiffened Compression Flanges [19]

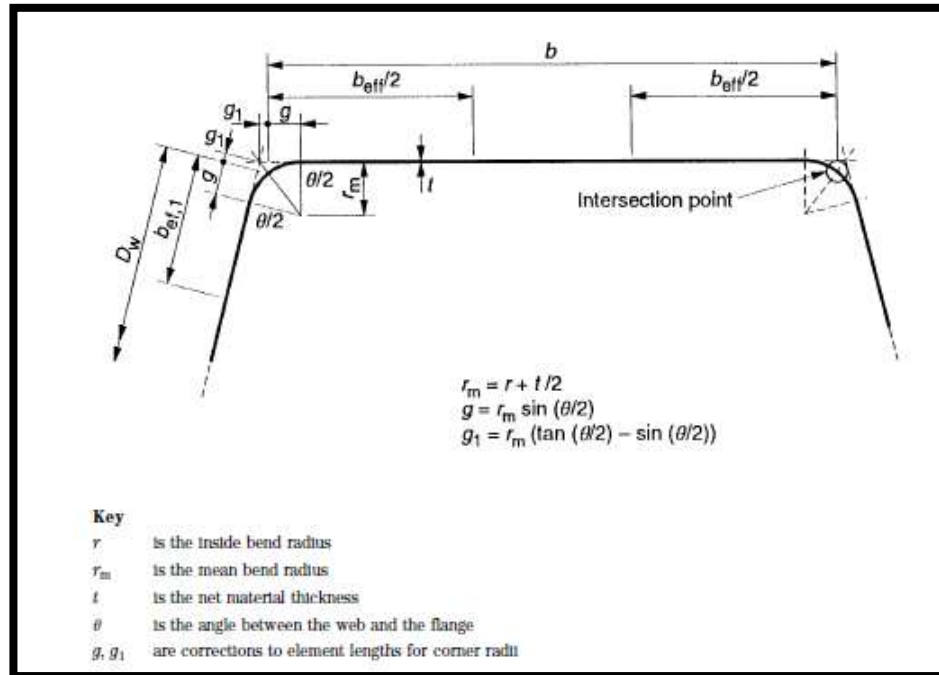


Figure 16: Calculation of Effective Widths Allowing for Corner Radii [19]

This study considered only the trapezoidal un-stiffened profiled sheet (which was provided by the supplier). The effective cross section of a trapezoidal sheeting profile, comprising of flat web elements and flat flange elements, as shown in Figure 17, should be determined as follows:

- a) The neutral axis should initially be located on the basis of fully effective webs, a fully effective tension flange and the effective width of compression flange determined in accordance with equation 3 using a compressive stress f_c equals to the design strength P_y .
- b) The effective widths of the webs should be determined.
- c) If the web is not fully effective, the position of the neutral axis may optionally be adjusted iteratively.

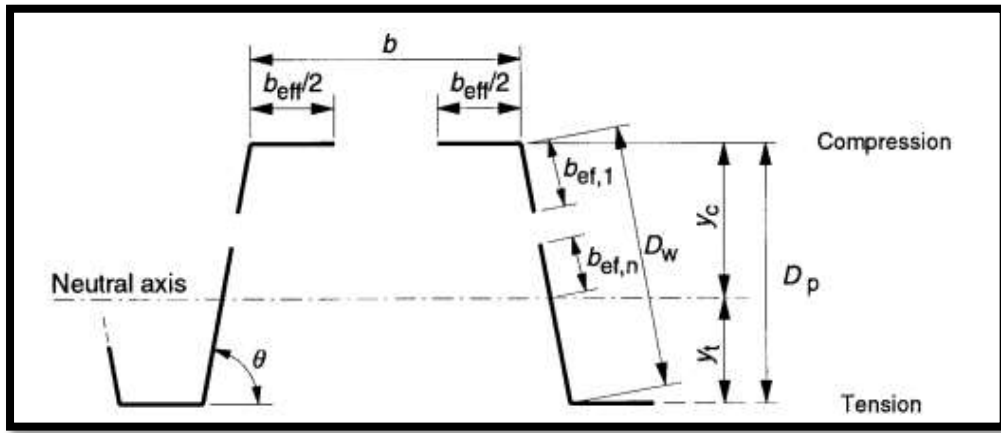


Figure 17: Effective Cross Section of an Unstiffened Trapezoidal Profile in Bending [19]

➤ Effective width of a flat unstiffened element:

➤ Flange

$$b_{eu} = 0.89 b_{eff} + 0.11b \quad (4)$$

where:

b_{eff} is determined from the basic effective width;

b is the flat width of the element.

The value of K may conservatively be taken (0.425) for any un-stiffened element. Alternatively a more precise value of K may be obtained from

$$K = 1.28 - \left(\frac{0.8h}{2+h} \right) - 0.0025h^2$$

where:

$$h = \frac{D_w}{b};$$

D_w is the sloping distance between the intersection points of a web and the flanges.

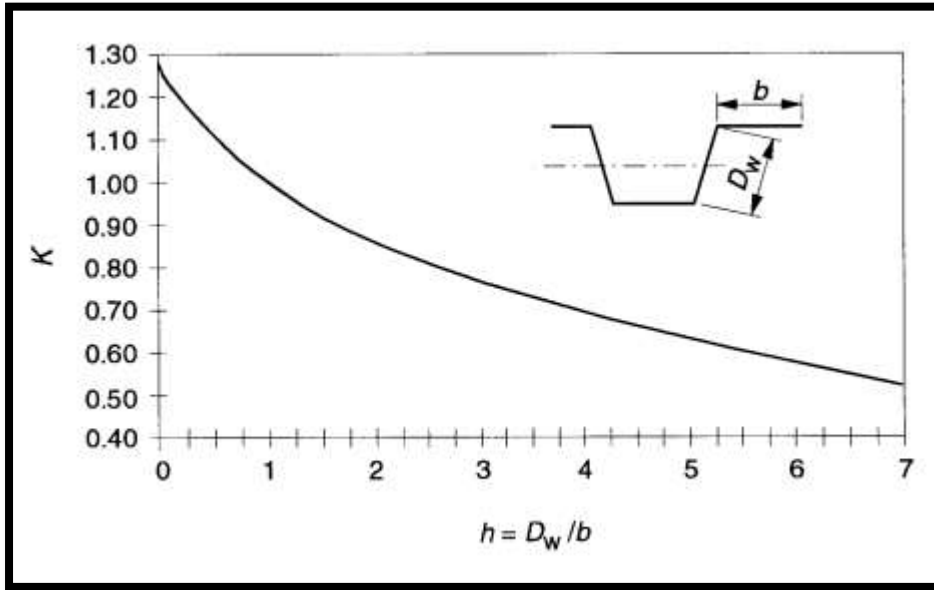


Figure 18: K Factors for Unstiffened Compression Flanges [19]

- Web: If the web depth to thickness ratio $D_w/t \leq 70\epsilon$ then it can be taken as fully effective. In all other cases the effective width of a web, in which the stress varies linearly, as shown in Figure 15, should be obtained in two portions, one adjacent to each edge as follows:

- a) Both edges in compression (see figure a):

$$b_{ef,1} = 0.76t \sqrt{E/f_{c,1}} \quad (5)$$

$$b_{ef,2} = (1.5 - (0.5f_{c,2}/f_{c,1}))b_{ef,1} \quad (6)$$

where:

$f_{c,1}$ is the larger compressive edge stress;

$f_{c,2}$ is the smaller compressive edge stress;

$b_{ef,1}$ is the portion of the effective width adjacent to the more compressed edge;

$b_{ef,2}$ Is the portion of the effective width adjacent to the less compressed edge;

E is the modulus of elasticity; t is the net thickness of the steel material. If $b_{ef,1} + b_{ef,2} \geq D_w$ the whole web is effective.

- b) One edge in tension (see figure b):

$$b_{ef,1} = 0.76t \sqrt{E/f_{c,1}} \quad (7)$$

$$b_{ef,3} = b_t + 1.5b_{ef,1} \quad (8)$$

where:

b_t is the width subject to tension;

$b_{ef,3}$ is the portion of the effective width adjacent to the tension edge.

If $b_{ef,1} + b_{ef,3} \geq D_w$ the whole web is effective (Figure 19).

c) Both edges in tension:

The whole web is effective. If the location of the neutral axis is determined iteratively, using effective section properties (rather than assuming the web to be fully effective), then $b_{ef,1}$ in items a) and b) above should be determined from $b_{ef,1} =$

$$0.95t \sqrt{\left(\frac{E}{f_{c,1}}\right)} \quad (\text{see Figure 19}).$$

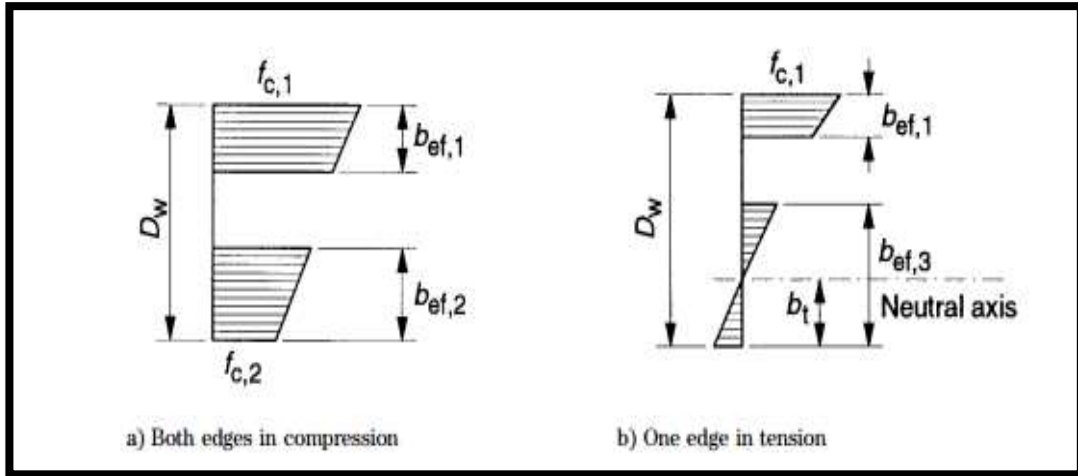


Figure 19: Stress Distributions Over Effective Portions of Web [19]

4.1.6 Design For Lateral Loading

A profiled steel sheet should be designed for lateral loading by verifying the resistance of a single profile to bending, shear and crushing, acting separately and in combination. This study focuses only on the bending moment because this study is trying to measure the resistance of the profiled sheets to uniform wind load. The wind load can be simulate as uniform load on the profiled sheet, Wind load create a bending moment on profiles.

4.1.7 Bending Moment Calculations for Steel Profiles

The effective cross section of a trapezoidal sheeting profile can be determined as follows:

- a) The neutral axis should initially be located on the basis of fully effective webs, a fully effective tension flange and the effective width of compression flange using a compressive stress f_c equal to the design strength p_y .
- b) The effective widths of the webs should be determined.
- c) If the web is not fully effective, the position of the neutral axis may optionally be adjusted iteratively.
- d) The moment capacity M_c should be determined as follows:

$$\text{If } y_c \geq y_t \quad : \quad M_c = p_y I_{eff} / y_c \quad (9)$$

where:

I_{eff} is the second moment of area of the effective cross section; y_c and y_t are as shown on (Figure 20).

If $y_c < y_t$ either:

- 1) Adopt the elastic stress distribution shown in Figure 20b in which the effective width of the compression flange b_{eff} is determined using a compressive stress f_c equal to the design strength p_y , then determine M_c from $M_c = p_y I_{eff} / y_t$
- 2) Adopt the stress distribution shown in Figure 20c in which b_{eff} is based on p_y and sufficient plasticity develops in the tension zone to permit f_c to reach p_y , adjusting the position of the neutral axis to maintain equilibrium between tension and compression on the effective cross section, and then determine M_c from the resulting stress diagram.

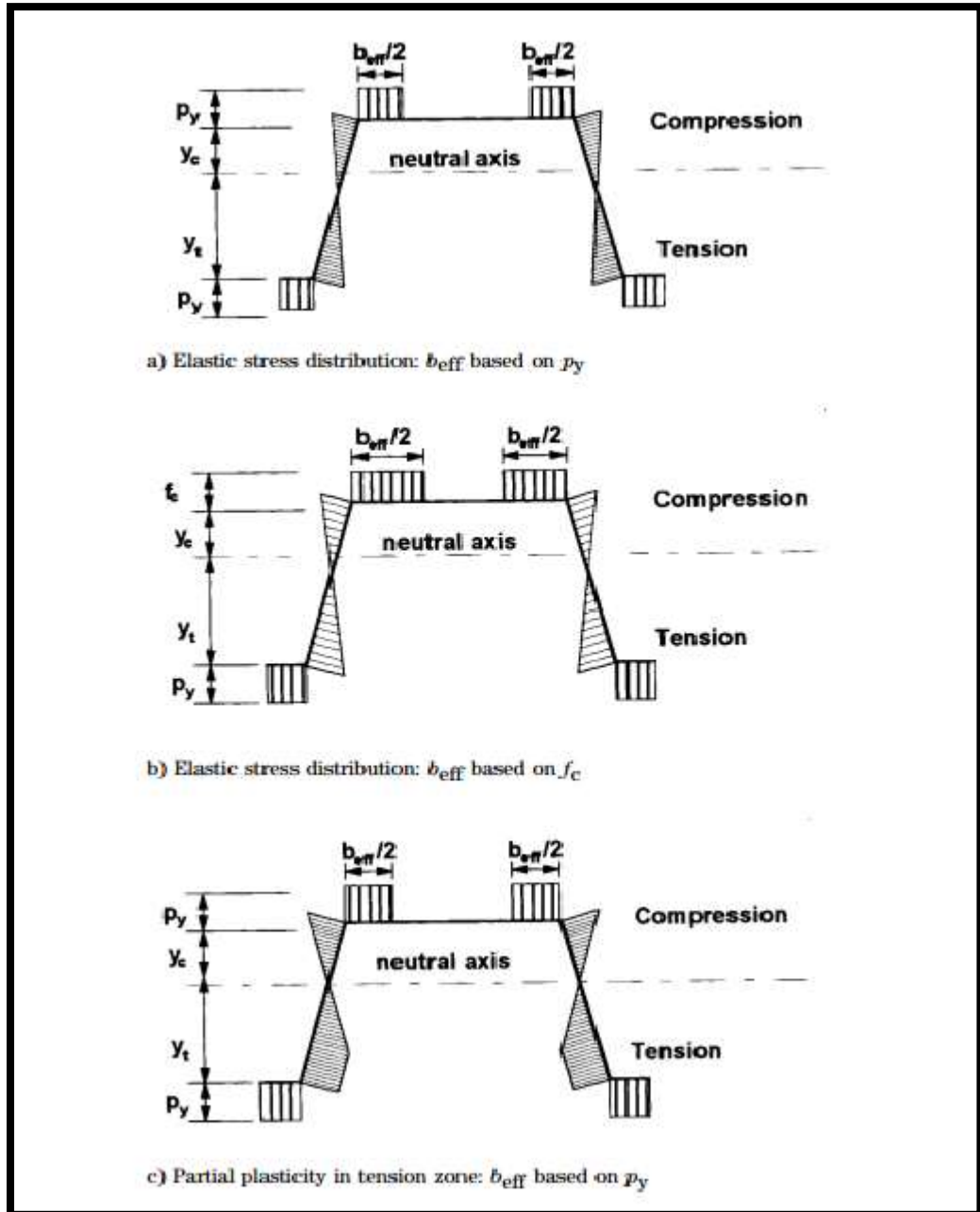


Figure 20: Alternative Methods for Determining the Moment Capacity when $y_c < y_t$ [19]

4.2 Design of Aluminum Cold Form Sheets

The steel and aluminum cold-formed sheets design is similar in many aspects but with some differences nonetheless. The main difference is in the concept of calculating the effective moment of inertia. In steel the effective moment of inertia is calculated based on the reduction in the area of the profile, as it was shown in the previous sections. However, the effective moment of inertia in aluminum profiles is calculated based on the reduction of the thickness of the profile. The design of cold-formed aluminum sheeting shall be following the general rules given in EN 1990 and

EN 1 999-1-1 [20]. Ultimate limit states and serviceability limit states should be multiplied by appropriate partial factors. The factors are used to increase capacity of the profile because these profiles are always connected to structures. The effect of structures should be taken into account because it increases the profile capacity as shown in Tables 3 and 4.

Table 3: Partial Factors for Ultimate Limit [20]

<i>Partial Factors For Ultimate Limit</i>	γ_x	value
resistance of cross-sections and members to instability	γ_{M1}	1.1
resistance of cross-sections in tension to fracture	γ_{M2}	1.25
resistance of joints	γ_{M3}	1.25

Table 4: Partial Factors for Serviceability Limit [20]

<i>Partial Factors For Serviceability Limit</i>	γ_x	Value
resistance of cross-sections and members to instability	γ_{M1}	1.0

4.2.1 Material Properties

(1) The characteristic values of 0.2 proof strength f_0 and tensile strength f_u have been obtained by adopting the values for minimum and $R_{p0.2}$ and R_m direct from the relevant product standards.

(2) It can be assumed that the properties in compression are the same in tension.

(3) If partially plastic moment resistance is used, the ratio of the characteristic ultimate tensile strength f_u to the characteristic 0.2 proof strength f_0 should be not less than 1.2.

(4) The material constants (modulus of elasticity etc.) should be taken as given in EN 1999-1-1 (see appendix A).

➤ Plane Cross- Section Parts Without Stiffeners

(1) The effective thickness t_{eff} of compression cross-section parts should be obtained as $t_{eff} = \rho * t$, where ρ is a reduction factor allowing for local buckling.

(2) The notional flat width b_p of a plane cross-section part should be determined as specified in the steel profiles design. Calculating of the cross-sections with sharp corners, using the following approximations:

$$A_g \cong A_{g,sh}(1 - \delta) \quad (10)$$

$$I_g \cong I_{g,sh}(1 - 2\delta) \quad (11)$$

where:

$$\delta = 0,43. (\sum_{j=1}^n (r_j \varphi_j / 90)) / \sum_{i=1}^m b_{p,i} \quad (12)$$

A_g is the area of the gross cross-section

$A_{g,sh}$ is the value of for a cross-section with sharp corners

$b_{p,i}$ is the notional flat width of plane cross-section part i for a cross-section with a corner shape

I_g is the second moment of area of the gross cross-section

$I_{g,sh}$ is the value of J_g for a cross-section with sharp comers

φ is the angle between two plane elements

m is the number of plane cross-section parts

n is the number of curved cross -section parts without consideration of the curvature of stiffeners in webs and flanges

r_j is the internal radius of curved cross-section part

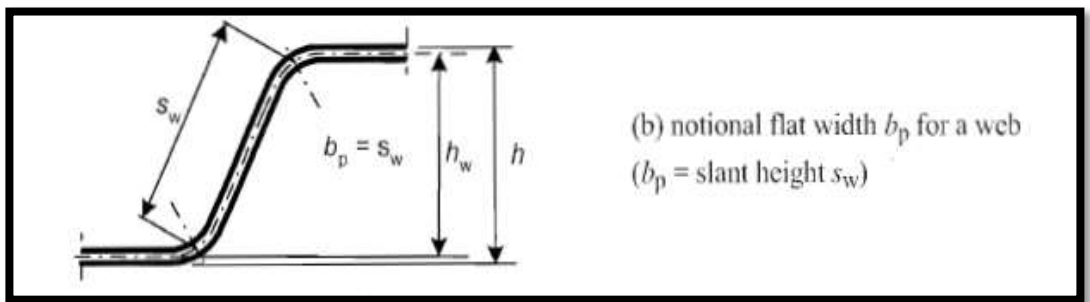


Figure 21: Notional Widths of Plane Cross-Section Parts b_p Allowing for Corner Radii [20]

- The reductions given in step (2) may also be applied in calculating the effective section properties A_{eff} and $I_{y,eff}$ provided that the notional flat

widths of the plane cross-section parts are measured to the points of intersection of their midlines.

(3) The reduction factor ρ used to determine t_{eff} should be based on the largest compressive stress $\sigma_{\text{com},Ed}$ in the relevant cross-section part (calculated on the basis of the effective cross section), when the resistance of the cross-section is reached.

(4) If $\sigma_{\text{com},Ed} = \frac{f_0}{\gamma_{M1}}$ the reduction factor ρ should be obtained from the following:

- If $\lambda_p \leq \lambda_{\text{lim}}$: $\rho = 1,0$
- If $\lambda_p > \lambda_{\text{lim}}$: $\rho = \alpha (1 - \frac{0.22}{\lambda_p})/\lambda_p$

In which the plate slenderness (λ_p) is given by:

$$\lambda_p = \sqrt{f_0/\sigma_{cr}} = \left(\frac{b_p}{t}\right) * \sqrt{\frac{12(1-\nu^2)*f_0}{\pi^2 EK \sigma}} \cong 1.052 \left(\frac{b_p}{t}\right) \sqrt{f_0/EK \sigma} \quad (13)$$

K_σ is the relevant bulking factor, it can be calculated from Table (6)

λ_{lim} and α can be taken from Table (5)

Table 5: Parameters λ_{lim} and α [20]

λ_{lim}	α
0.517	0.90

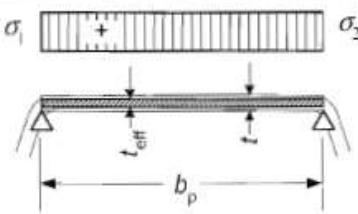
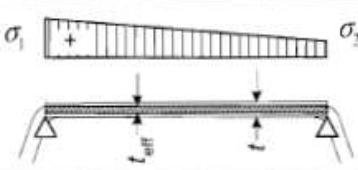
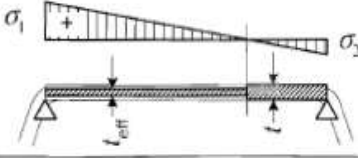
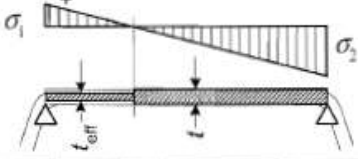
(5) In determining the effective thickness of a flange cross-section part subject to stress gradient, the stress ratio φ used in Table 6 may be based on the properties of the gross cross-section.

(6) In determining the effective thickness of a web cross-section part the stress ratio φ used in Table 6 can be obtained using the effective area of the compression flange but the gross area of the web.

4.2.2 Design of Aluminum of Profiled Sheets

(1) The cross-section of an intermediate stiffener should be taken as comprising the stiffener itself plus the adjacent effective portions of the adjacent plane cross-section parts $b_{p,1}$ and $b_{p,2}$ shown in Figure 22.

Table 6: Buckling coefficient K_σ for cross-section parts in compression [20]

Cross-section part (+ = compression)	$\psi = \sigma_2 / \sigma_1$	Buckling factor k_σ
	$\psi = +1$	$k_\sigma = 4,0$
	$+1 > \psi \geq 0$	$k_\sigma = \frac{8,2}{1,05 + \psi}$
	$0 > \psi \geq -1$	$k_\sigma = 7,81 - 6,26\psi + 9,78\psi^2$
	$-1 > \psi \geq -3$	$k_\sigma = 5,98(1 - \psi)^2$

➤ The procedure, which is shown in Figure 22 on the following page, should be carried out in the following steps:

- (1) All initial effective cross-section for the stiffener should be found to calculate the cross-section area A_s . Using effective thickness determined by assuming that the stiffener is longitudinally supported and that $\sigma_{con,ed} = f_0/\gamma M_1$ Using another effective cross-section of the stiffener to calculate the effective second moment of inertia in order to determine the reduction factor for distortional buckling, allowing for the effects of the continuous spring restraint.

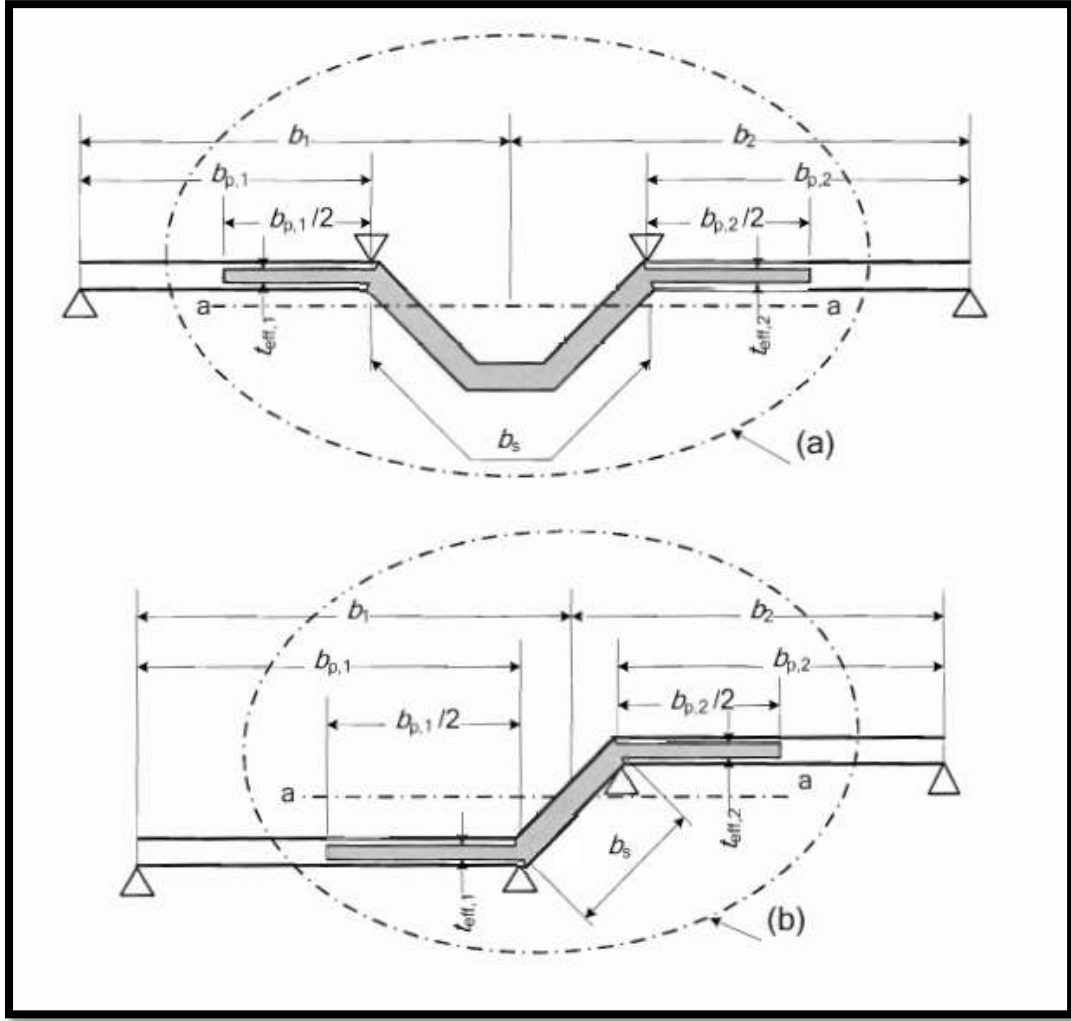


Figure 22: Initial Effective Cross-Section Area A_s for Intermediate Stiffeners in (a) Flange and (b) Web [20]

- Optionally iterate to refine the value of the reduction factor for buckling of the stiffener.
- (2) Initial values of the effective thickness $t_{eff,1}$ and $t_{eff,2}$ shown in Figure 22 are determined by assuming that the plane cross-section part $b_{p,1}$ and $b_{p,2}$ are doubly supported.
- (3) The effective cross-sectional area of an intermedia stiffener as should be obtained from:

$$A_s = \left(\frac{t_{eff,1} \cdot b_{p,1}}{2} \right) + (t \cdot b_s) + \left(\frac{t_{eff,2} \cdot b_{p,2}}{2} \right) \quad (14)$$

where:

b_s is the stiffener width (Figure 18).

- (4) The critical buckling stress $\sigma_{cr,s}$ for an intermediate stiffener can be obtained from:

$$\sigma_{cr,s} = \frac{2\sqrt{KEI_s}}{A_s} \quad (15)$$

where:

K is the spring stiffness per unit length.

I_s is the effective second moment of area of the stiffener, using the thickness t and notional effective width l_2t of adjacent plane cross-section parts about the centroid axis a-a of its effective cross-section, (Figure 20(a)).

- (5) The reduction factor χ_d for the distortional buckling resistance of an intermediate stiffener can be obtained from the value of using Table 7.

Table 7: Reduction Factor χ_d [20]

λ_s	χ_d
$\lambda_s \leq 0.25$	1.0
$0.25 < \lambda_s < 1.04$	$1.155 - 0.62\lambda_s$
$1.04 \leq \lambda_s$	$0.53/\lambda_s$

$$\triangleright \lambda_s = \sqrt{f_0/\sigma_{cr,s}}$$

- (6) If $\chi_d < 1$ it may optionally be refined iteratively, starting the iteration with modified values of ρ obtained with $\sigma_{com,Ed}$ equal to $\frac{\chi_d f_0}{\gamma_{M1}}$, so that:

$$\triangleright \lambda_{p,red} = \lambda_p \sqrt{\chi_d}$$

- (7) If iteration is carried out, it should be continued until the current value of χ_d is approximately equal to, but not more than, the previous value.
- (8) The reduced effective area of the stiffener $A_{s,red}$ allowing for distortional buckling should be taken as:

$$A_{s,red} = \chi_d A_s \frac{f_0/\gamma_{M1}}{\sigma_{com,Ed}} \quad \text{But } A_{s,red} \leq A_s$$

where $\sigma_{com,Ed}$ is compression stress at the centerline of the stiffener calculated on the basis of the effective cross-section.

- (9) In determining the effective section properties, the reduced effective area $A_{s,red}$ should be represented by using a reduced thickness $t_{red} = \chi_d t_{eff}$ for all the cross-section parts included in A_s .

➤ Calculating bending moment:

- Elastic and elastic-plastic resistance with yielding at the compressed flange:

(1) The design moment resistance of a cross-section for bending $M_{c,Rd}$ should be determined as follows:

- If the effective section modulus W_{eff} is less than the gross elastic section modulus W_{el} :

$$M_{c,Rd} = W_{eff} f_0 / \gamma_{M1}$$

- If the effective section modulus W_{eff} is equal to the gross elastic section modulus W_{el} :

$$M_{c,Rd} = f_0 (W_{el} + (W_{pl} - W_{el}) 4(1 - \frac{\lambda}{\lambda_{el}})) / \gamma_{M1} \quad (16)$$

But not more than

$$W_{pl} f_0 / \gamma_{M1}$$

where:

λ Is the slenderness of the cross-section part which corresponds to the largest value of λ/λ_{el} ;

For double supported plane cross-section part $\lambda = \lambda_p$ and $\lambda_{el} = \lambda_{lim}$ where λ_{lim} is shown in Table (7). For stiffened cross-section part $\lambda = \lambda_s$ and $\lambda_{el} = 0.25$.

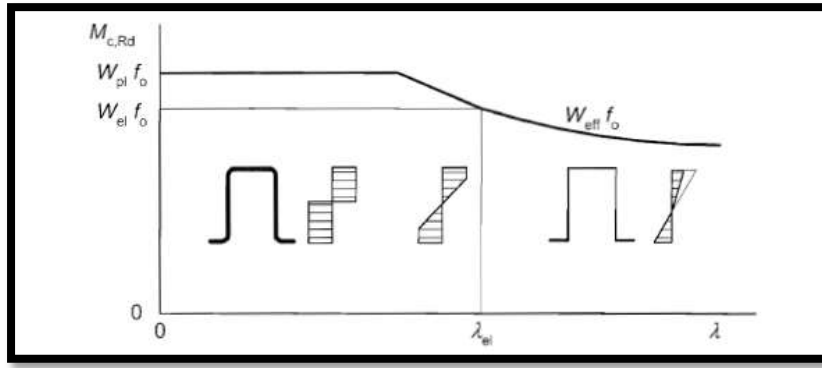


Figure 23: Bending Moment Resistance as a Function of the Slenderness [20]

(2) Equation (16) is valid the slope of the web relative to the flanges is less than (60°).

(3) If step (2) is not fulfilled the following equation should be used:

$$M_{c,Rd} = W_{el} f_o / \gamma_{M1}$$

(4) The effective section modulus W_{eff} should be based on an effective cross-section that is subject only to bending moment, with a maximum stress $\sigma_{max,Ed}$ equal to f_o / γ_{M1} , allowing for the effects of local and distortional buckling. Where shear lag is relevant, allowance should also be made for its effects.

(5) The stress ratio $\psi = \frac{\sigma_2}{\sigma_1}$ used to find the effective portions of the web can be calculated by using the effective area of the compression flange but the gross area of the web (Figure 24).

(6) If yielding happens first at the compression side of the cross-section, and the profile does not yield at the tension flange only the value of W_{eff} should be based on a linear distribution of stress across the cross-section.

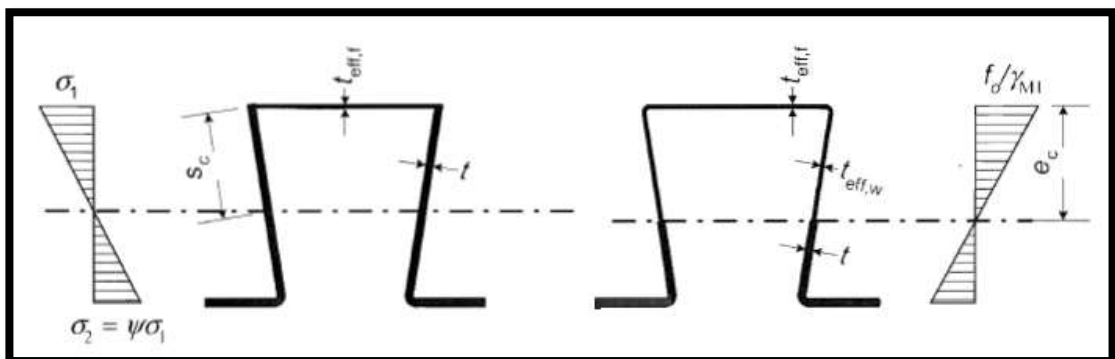


Figure 24: Effective Cross-Section for Resistance to Bending Moments [20]

➤ Elastic and elastic-plastic resistance with yielding at the tension flange only:

- (1) If the yielding happens first at the tension side, plastic reserves in the tension zone can be used without any strain limitation until the maximum compressive stress $\sigma_{com,Ed}$ reaches f_0/γ_{M1} . In this cause only the bending case is considered.
- (2) In this case, the effective partially plastic section modulus $W_{pp,eff}$ should be based on a stress distribution that is bilinear in the tension zone but linear in the compression zone.
- (3) In the absence of a more detailed analysis, the effective thickness t_{eff} of the webs may be obtained by basing e_c on the bilinear stress distribution (Figure 25), by assuming $\psi = -1$.

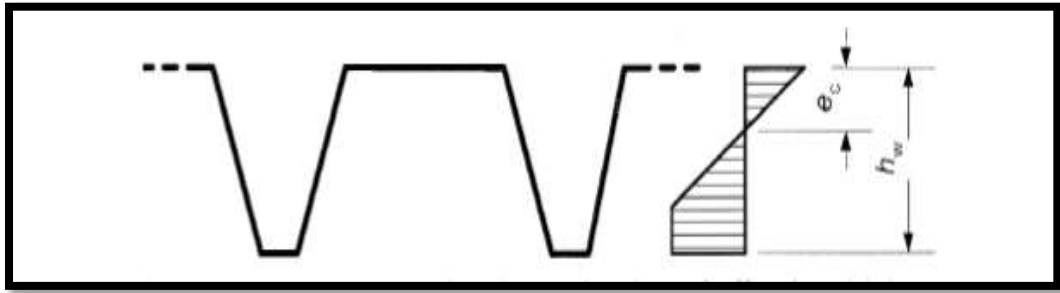


Figure 25: Measure e_c for Determination of Effective Thickness [20]

4.3 Testing Method

This research has introduced a set up that simulates the respective wind and snow load (uniform load) accurately. Moreover, the set-up is built from good quality materials and very accurate measurement devices. Furthermore, the set-up is a simple testing method that used by any semiskilled workers.

The set-up, involved creating a stand with four steel legs with the following dimensions: 2.5m x 2.5m *width* x 1m *height* and 6mm *thickness*. These four legs where connected by two rectangles beams as shown in (Figure 26) the dimensions of the rectangular stands is 2.5 m X 1.5m X 0.2 m height. The top rectangle (Figure 27) is height adjustable, it can move up and down so that the machine can test different profiles with different heights.

A deflection laser sensor was fixed to measure the respective deflection of the profiled steel sheet, the laser was fixed in the center of the set up were the maximum deflection is expected. This sensor can record the deflection of the sheet under the load pressure with time. The (optoNCDT 1700) laser displacement sensor was chosen for this study. This sensor has many features such as, the unique Real-Time Surface

Compensation (RTSC) feature, which enables measurement against a wide range of material surfaces. Its unique compact design makes it ideal for all industrial applications, its measuring range is (200 mm) which is more than the deflection limit expected (100mm) (Figures 28 and 29).

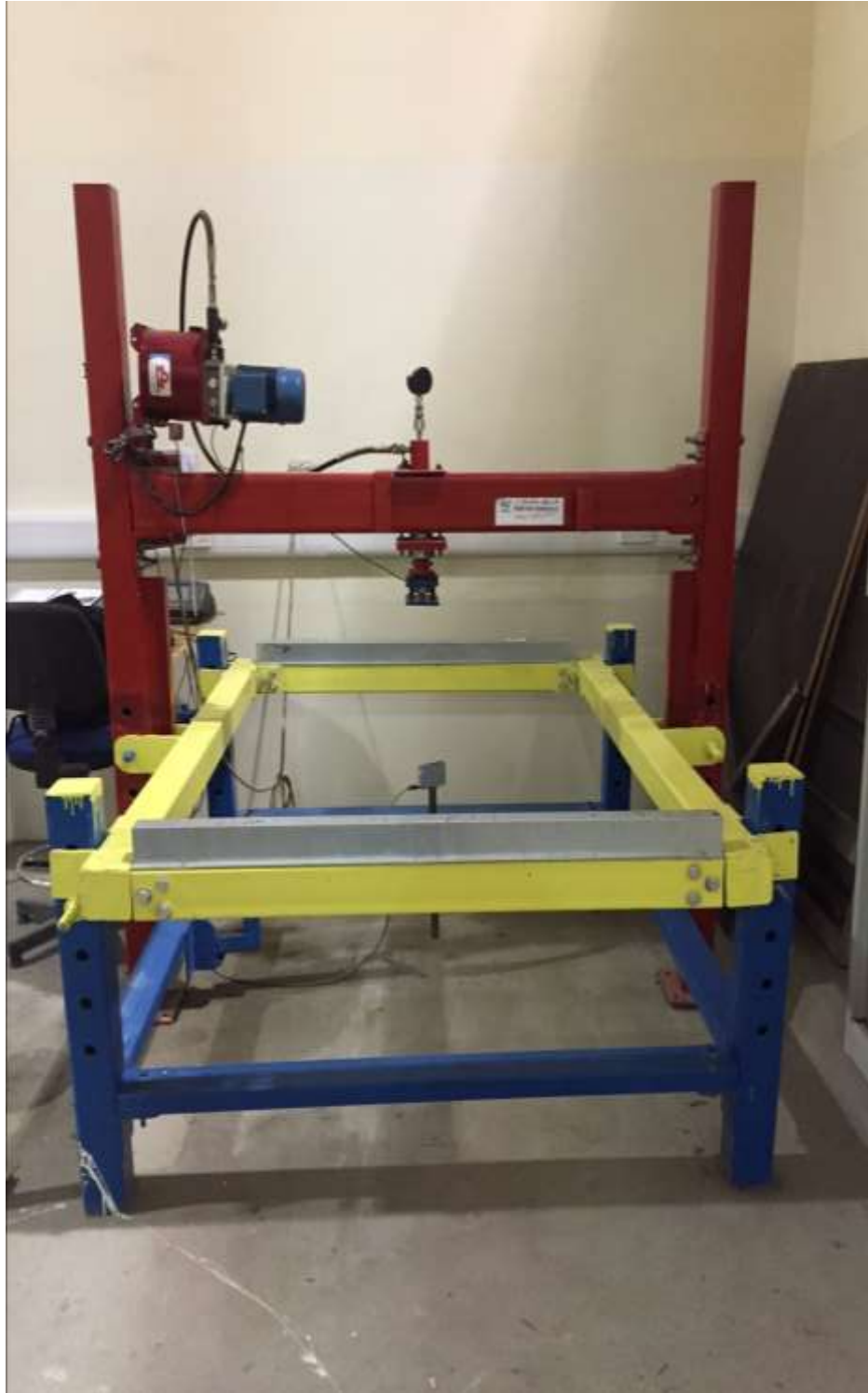


Figure 26: Testing Setup

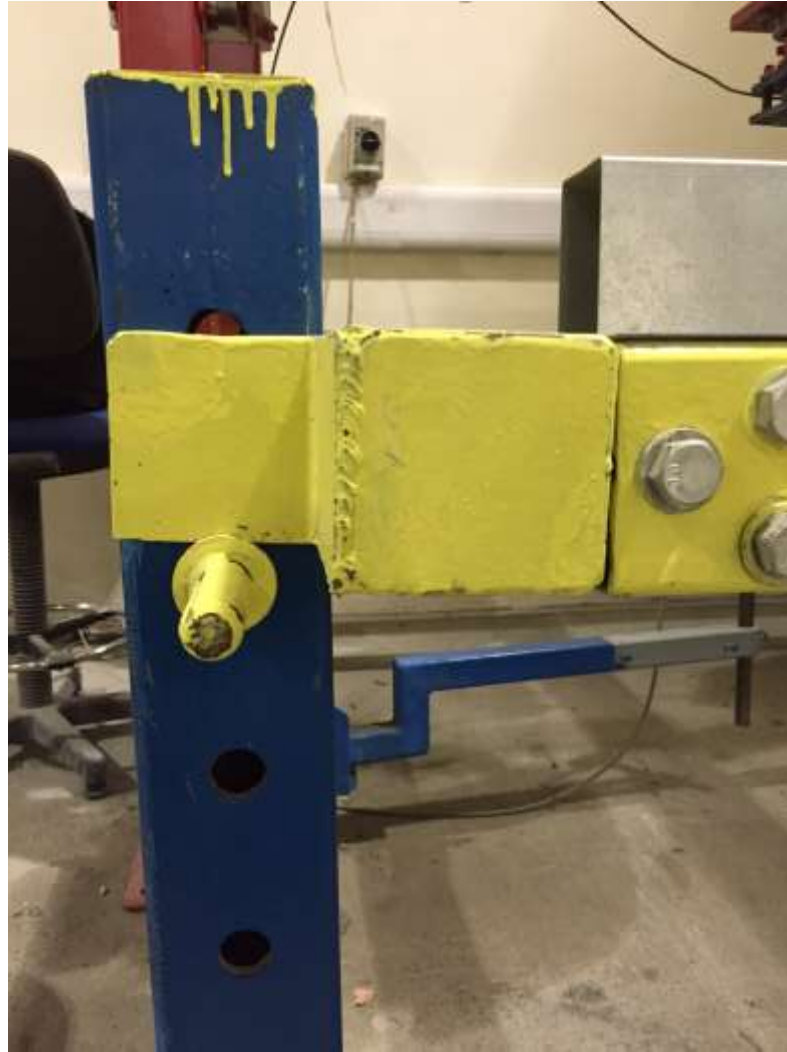


Figure 27: Adjustable Legs



Figure 28: OptoNCDT 1700 Laser Sensor



Figure 29: Laser Sensor Location in the Frame

On top of the profiled steel sheet, an air mattress is placed to distribute the load uniformly over the profiled sheet. Wooden plate is placed on the top of the air mattress which is followed by a steel rectangle to guarantee a uniform distribution for the load over the profiled sheet. This steel rectangle is attached to a loading jack (Figure 30). The mini power pack center block C/299 was chosen to apply the needed jacking force for testing the profiled sheets. This hydraulic piston is made with high pressure die casting process which gives the block excellent precision and makes it good for industrial use. The standard version is intended for single and double acting applications, in this study a single acting was chosen because the load will be applied from one direction. Single acting provides the necessary oil flow to the pressure line when the motor is running, elevating the load. Once the motor is stopped, the block maintains the pressure in the cylinder. The movement of the cylinder is produced when the built-in electro valve is activated (Figures 30 and 31).



Figure 30: Cell Load and Piston



Figure 31: Hydraulic Pump

A load cell was installed to measure the applied load. A most popular general-purpose compression load cell is the PT cell load. PTX load cell was chosen because of its unique design.

All electronics components are housed through the bottom of the load cell, which is protected against external damage. It is suitable for tank, hopper, silo work and all industrial-weighing projects. It is also covered with a corrosion resistant anodizing or electrodes nickel plate, which makes it perfect for hostile environments. (LPX-5000kg) was used in the machine so that it can measure the load of all the profiles with 0.1% linearity error (Figures 32 and 33).



Figure 32: Load Cell



Figure 33: Load Cell Display Device

Both the load cell and the laser sensor is connected to a computer and the reading is recorded separately. However, the recording time intervals differ, they are different for the laser and the load cell which makes it difficult to draw a graph directly from the recording. The reading for different tests does not begin from zero, therefore; the reading should be adjusted for this error. Using an Excel program makes all the first reading start from zero by subtract the first un-useful reading from the record. Furthermore, the set-up was verified and calibrated by testing three profile (38/200 GI 0.7) and compared their result with the calculated ones.



Figure 34: Loading Control Panel

Figure 35 shows the complete set up, and demonstration how the load will be distrusted from a point load to a uniform load. Moreover, Figure 35 demonstrates how all the components are connected to the frame.



Figure 35: Full Loading Setup

4.4 Modeling by Finite Element

The profile of the model selected for the study was trapezoidal and the dimensions are adopted from commercially available plates. The geometry of the corrugated plate is given in Figure 36. The variations in the parameters adopted for the numerical analysis are tabulated in Table 8.

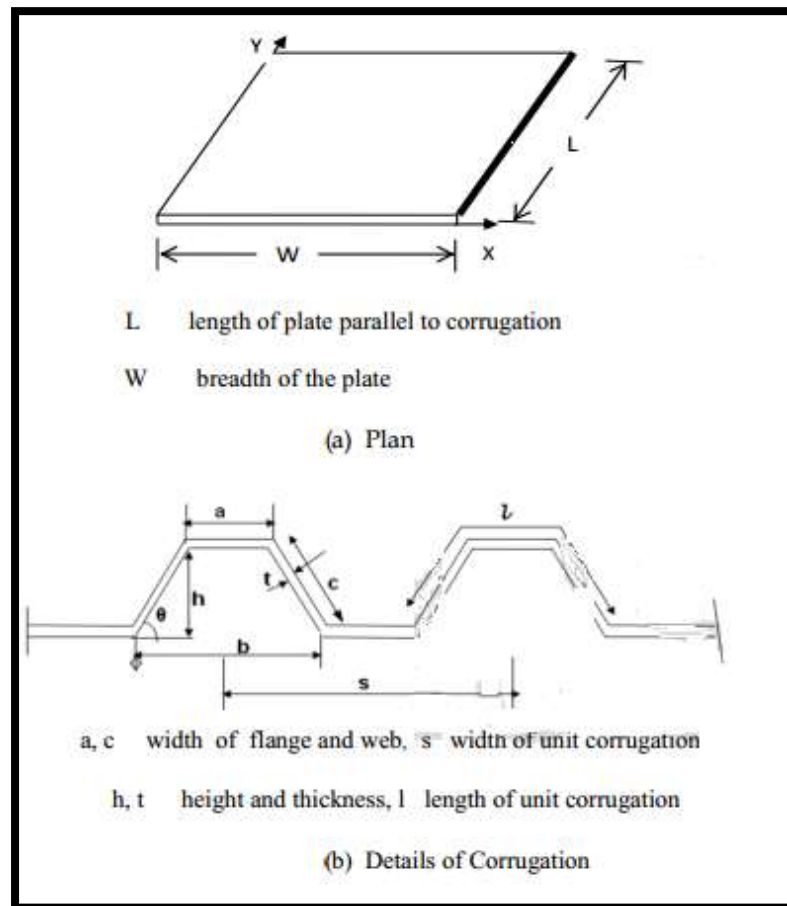


Figure 36: FE Model

The finite element method has been used in the present study to determine the critical elastic buckling load for the profiled steel sheets. The program ABACUS® satisfied all those items.

Shell Elements

In order to see the difference in performance of the profiled sheet, when including local buckling, a model with shell elements was made. A model with shell elements includes the cross section in the analyses, and the behavior of the cross section, during the load application, is shown Figure 37. These are typically “planar” elements, they are used to model thin structures which will experience bending. It is difficult to model thin structures with 3-D elements, because many nodes are needed through thickness to capture bending behavior (Figure 37), therefore, shell element was used in the model.

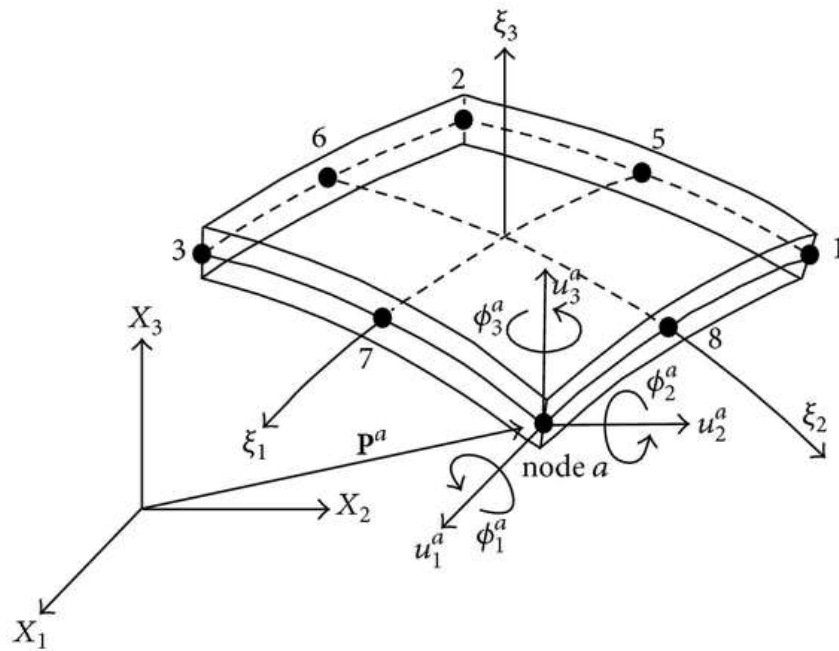


Figure 37: Geometry of 8-node Shell Element with Six Degrees of Freedom [21].

Geometry

The geometry of shell elements can be made in different ways. For this sheet model the shell tool sweep was used. When using sweep a path representing the length and position of the member is first created, similar to the path line for beam elements as shown in Figure 38.

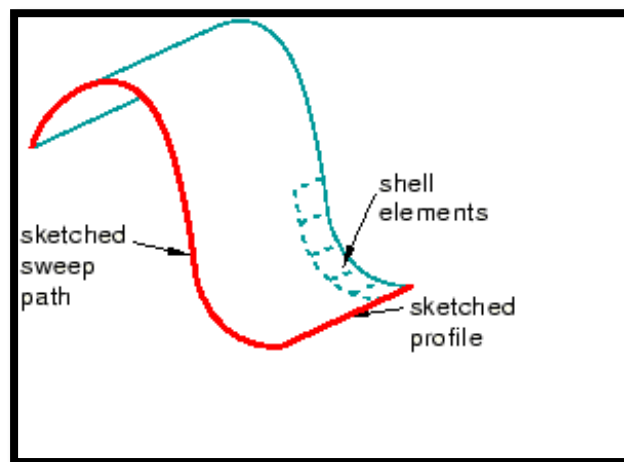


Figure 38: Sweep Action [21]

Moreover, using the beam path will create the effect of the profiling to the metal sheets. As for the path line for beam elements, the exact coordinates for the path can be entered which makes it easier when assembling the members into a model. However, assembling the member by moving them into their exact position, can also be created. The sheet exact coordinates were given to the paths since all the members have different angles and it would be difficult to move the members into their right position during the assembly (Figure 39). When the path is created, a line representing the cross section is drawn. A thickness is thereafter assigned to this line. This thickness should represent the thickness of the cross section for the steel member and it could be assigned in different ways. The thickness could originate from the right side, left side, from the middle of the cross section line, or a specific point could be entered in section assignment. For the sheet, the origin of the thickness of the line representing the cross section, was chosen to be in the middle. The choice was based on the ease to understand the location and appearance of the cross section. During the assembling it is important to keep in mind the location of the origin line in the cross section, since this is the line displayed in the model and not the thicknesses of each part in the cross section. In the beam model, simplifications of the supports were made.

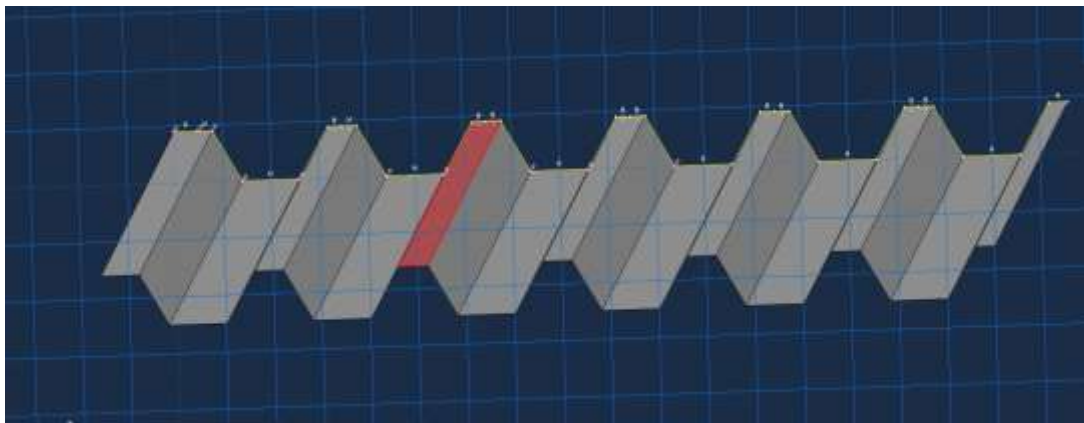


Figure 39: Beam Behavior in the Model

Properties

Isotropic thin shell elements, the QSI4 thin shell element, from the LUSAS-FE element library, was chosen for this purpose. The QSI4 element has four nodes and six

degrees of freedom per node. The input properties into the finite element model, such as the geometry and dimensions of the components (Table 8), and the Young's modulus, were taken from the manufacturers' details (205,000 N/mm²). The Poisson's ratios are assumed to be 0.35.

Table 8: The Plate Dimension in the FE Model

Element	Values
<i>Length (L)</i>	<i>2000 (mm)</i>
<i>Thickness of Plate (t)</i>	<i>0.6-0.7 (mm)</i>
<i>Angle of Inclination (θ)</i>	<i>45</i>
<i>Height (h) (mm)</i>	<i>38</i>
<i>Flange (a) (mm)</i>	<i>30</i>

Load Application

When modelling with shell elements, it is possible to apply the load on a surface, line or node. The load for this sheet is applied as a pressure load acting on the top surface. In order to be able to compare the model with the tested value and the calculated value, a deflection limit of 22.22 mm (L/90) was assigned to the model. When the deflection of the profiled sheet reached this limit, it is consider a failure in the sheet.

Boundary Conditions

Boundary conditions can be defined on surfaces, lines or nodes when modelling with shell elements. The profiled sheet, with shell elements, was modelled as simply supported. The lower nodes of the cross section of the profile on both sides of the sheet were locked in all three directions, but free in rotations. To simulate the bending test of the profiled sheets, the boundary conditions were assigned at intervals of 200mm, considering the total width of the profile to be 950mm.

Chapter 5: Results and Discussion

In this study, 47 samples were tested under uniform loads created by the machine to evaluate the proposed testing method and compare it with theoretical data to check the accuracy of the proposed set-up. Two types of material were used, steel and aluminum, with different profiles and different thicknesses. Tables 9 and 10 show the profile of each material with their measured thicknesses. A micrometer caliper was used to measure the thickness of the profiled sheet (Figure 40a), the value was adjusted by subtracting the thickness of the paint (the paint thickness was measured using a coating thickness meter (Figure 40b)).



Figure 40: a) Micrometer Caliper b) Coating Thickness Meter

The coding of the profile is different from one manufacture to another. In this study, the coding was according to the Middle East Insulation (MEI) (38 is the height of the mountain and 200mm is the distance between two consecutive mountains) (Figure 41).

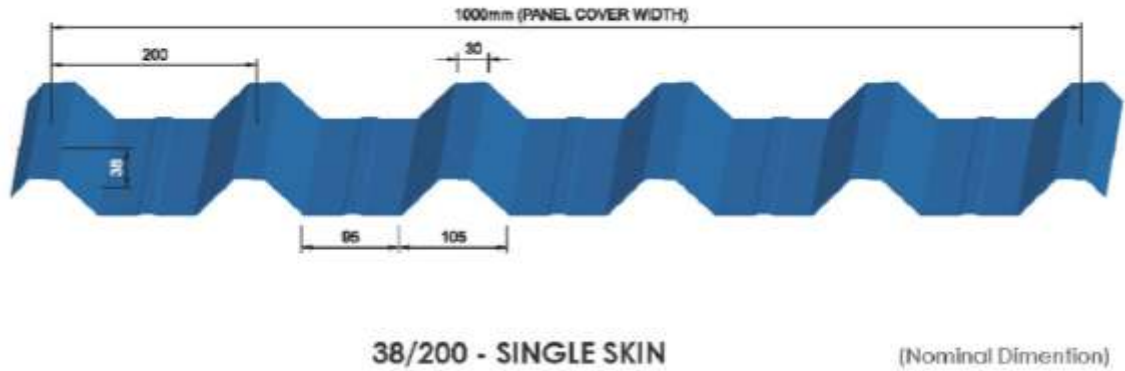


Figure 41: Steel Sheet Profiles of MEI

All the samples were tested under the same testing conditions. All the sheets were fixed in both directions to simulate the real application. The rate of the loading was adjusted for each thickness so that the test time ranges from two to twenty minutes. For thicker profiles, the loading rate is increased so that the time required to reach failure matches thinner profiles. Long term effects, such as creep, may increase deflection. In most cases the failure was in the middle of the sheet as shown in Figures 42 and 43, because the maximum deflection is expected in the middle.



Figure 42: Local Buckling in the Profiled Sheet



Figure 43: Local Buckling

From the set-up two values were obtained, one is the deflection using the laser sensor which was fixed in the center beneath the metal profile and the second one was the load that was measured using a load cell fixed in the piston. The measuring interval for the laser sensor and the load cell were not the same. Therefore, a program using excel was used to adjust the two timings. In the present study, the moment of inertia of the profile was calculated by assuming the profile as a beam behavior. By calculating the moment of inertia to the profile it took into account the changes in the effective dimensions, which effect the strength of the profile, as it was shown the methodology. After finding the values of the moment of inertia, the bending moment can be calculated from the following equation.

$$\sigma = \frac{My}{I}$$

Table 9: Steel Sheet Profiles Type and Thicknesses

Item	Material type (steel)	Profile type	Measured thickness (mm)
1	GI	32/250	0.634
2	GI	32/250	0.645
3	GI	45/150	0.642
4	GI	45/150	0.652
5	GI	45/150	0.661
6	GI	38/200	0.619
7	GI	38/200	0.622
8	GI	38/200	0.6235
9	GI	38/200	0.624
10	GI	38/200	0.6243
11	GI	38/200	0.6249
12	GI	38/200	0.626
13	GI	38/200	0.635
14	GI	38/200	0.641
15	GI	38/200	0.645
16	GI	38/200	0.648
17	GI	45/150	0.42
18	GI	45/150	0.437
19	GI	45/150	0.4548
20	GI	38/200	0.71
21	GI	38/200	0.73
22	GI	38/200	0.74
23	GI	38/200	0.4398
24	GI	38/200	0.4488
25	GI	38/200	0.455
26	GI	45/150	0.82
27	GI	45/150	0.829
28	GI	45/150	0.835

Source: Profiles from Middle East Insulation

Item	Material type (aluminum)	Profile	Measured thickness (mm)
-------------	---------------------------------	----------------	--------------------------------

1	Table 10: Aluminum Sheet Profiles Type and Thicknesses		
2	AL	45/250	0.673
3	AL	32/250	0.69
4	AL	45/150	0.638
5	AL	45/150	0.645
6	AL	45/150	0.648
7	AL	45/150	0.668
8	AL	38/200	0.75
9	AL	38/200	0.75
10	AL	38/200	0.755
11	AL	38/200	0.758
12	AL	38/200	0.773
13	AL	38/200	0.8456
14	AL	38/200	0.85
15	AL	38/200	0.86
16	AL	38/200	0.885
17	AL	38/200	0.89
18	AL	38/200	0.492
19	AL	38/200	0.5

Source:
Profiles
from
Middle
East

Insulation

Equation (17) was used to calculate the deflection for a rectangular beam under a uniform load. The proposed machine measured two values: the deflation (Δ) and the point load W as shown in Figure 44. After plotting deflection vs. load, the slope of the resulting figure had been multiplied by a constant value to find the moment of inertia. Then, using the moment of inertia, the stress can be calculated.

$$\Delta = \frac{5 * W * L^3}{384EI} \quad (17)$$

$$W = w * L$$

$$\Delta = \frac{5 * w * L^4}{384EI}$$

$$\text{Slope} = \frac{W}{\Delta}$$

where:

$$EI = \text{Slope} * \frac{5L^4}{384}$$

$$I = \text{Slope} * \frac{5L^4}{384E}$$

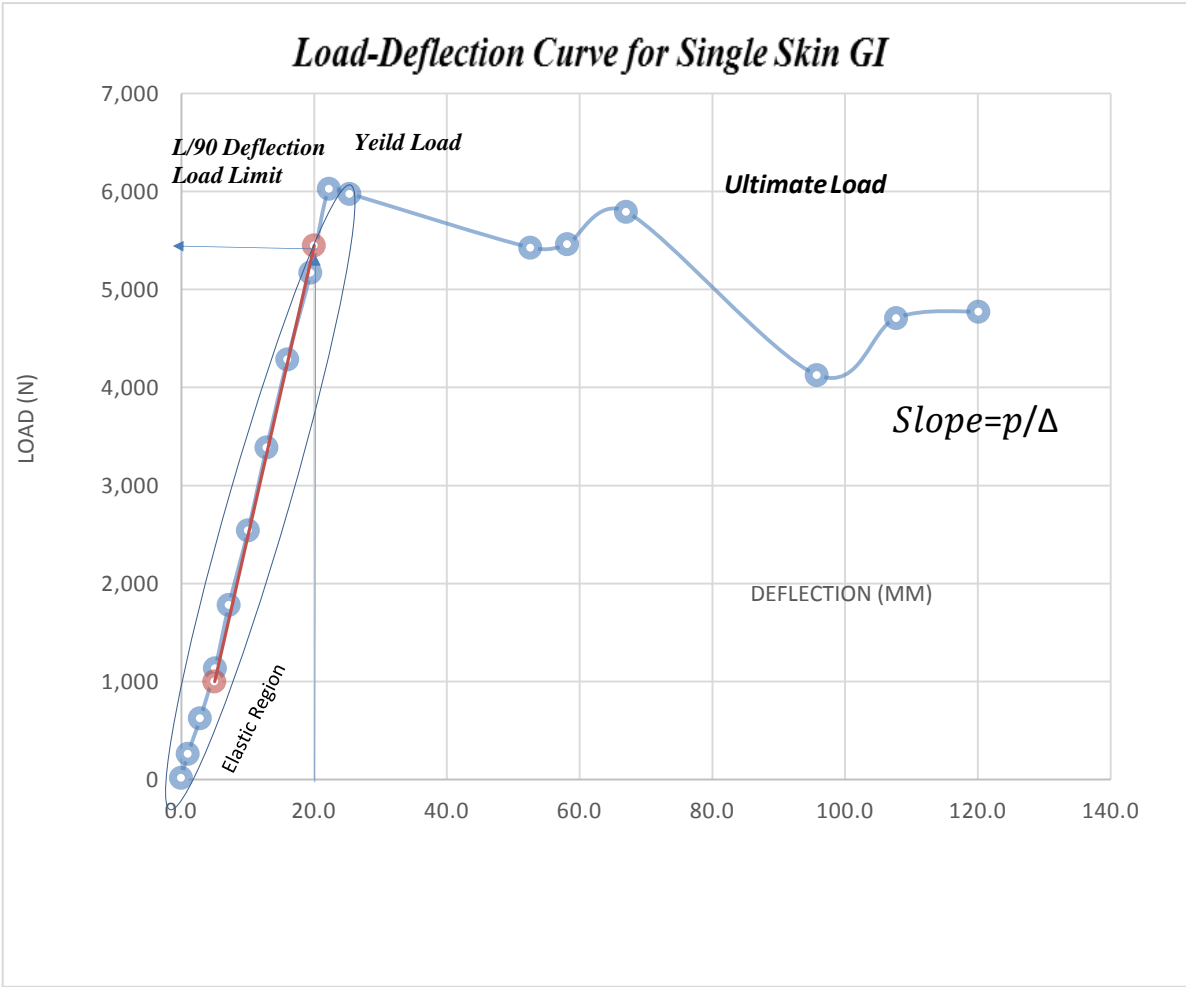
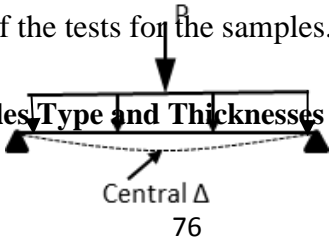


Figure 44: Graph of the Moment of Inertia

Table 11 shows the result of the tests for the samples.

Table 11: Steel Sheet Profiles Type and Thicknesses and Their Tested Moment



Item	Material type (steel)	Profile	Measured thickness (mm)	Moment of inertia (mm⁴/ m width) (tested)
1	GI	32/250	0.634	89,770
2	GI	32/250	0.645	86,112
3	GI	45/150	0.642	242,207
4	GI	45/150	0.652	261,826
5	GI	45/150	0.661	262,826
6	GI	45/250	0.619	136,287
7	GI	45/250	0.622	138,581
8	GI	45/250	0.6235	137,449
9	GI	38/200	0.624	137,703
10	GI	38/200	0.6243	141,832
11	GI	38/200	0.6249	141,006
12	GI	38/200	0.626	139,358
13	GI	38/200	0.635	142,276
14	GI	38/200	0.641	140,260
15	GI	38/200	0.645	146,087
16	GI	38/200	0.648	147,789
17	GI	45/150	0.42	144,416
18	GI	45/150	0.437	150,433
19	GI	45/150	0.4548	160,462
20	GI	38/200	0.71	153,252
21	GI	38/200	0.73	159,552
22	GI	38/200	0.74	156,504
23	GI	38/200	0.4398	92,387
24	GI	38/200	0.4488	95,274
25	GI	38/200	0.455	96,545
26	GI	45/150	0.82	338,753
27	GI	45/150	0.829	333,753
28	GI	45/150	0.835	336,753

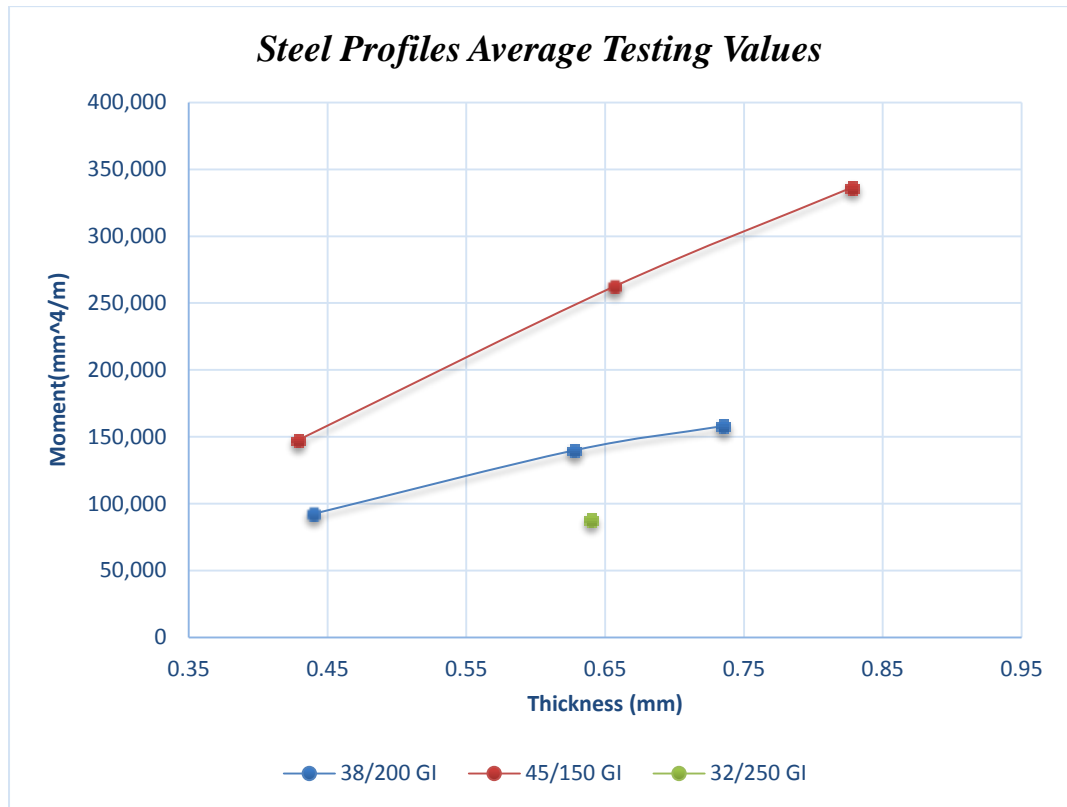


Figure 45: Steel Profiles Averaged Testing Values for Different Profiles

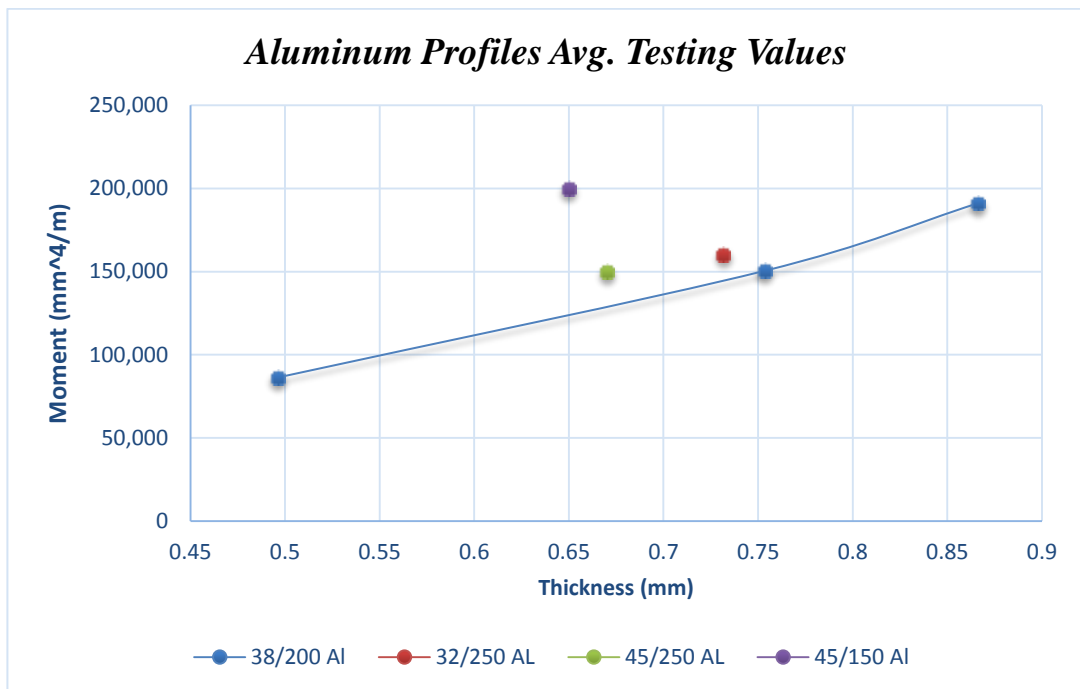


Figure 46: Aluminum Profiles Averaged Testing Values for Different Profiles

Table 12 shows the moment of inertia of the aluminum profiles with different thicknesses.

Table 12: Aluminum Sheet Profiles Type and Thicknesses and Their Tested Moment

Item	Material type (aluminum)	Profile	Measured thickness (mm)	Moment of inertia (mm ⁴ / m width) (tested)
1	AL	45/250	0.667	143,703
2	AL	45/250	0.673	155,896
3	AL	32/250	0.69	160,481
4	AL	45/150	0.638	198,413
5	AL	45/150	0.645	195,802
6	AL	45/150	0.648	191,327
7	AL	45/150	0.668	213,033
8	AL	38/200	0.75	148,809
9	AL	38/200	0.75	144,461
10	AL	38/200	0.755	151,785
11	AL	38/200	0.758	156,250
12	AL	38/200	0.773	159,970
13	AL	38/200	0.8456	184,796
14	AL	38/200	0.85	183,150
15	AL	38/200	0.86	189,112
16	AL	38/200	0.885	197,421
17	AL	38/200	0.89	200,321
18	AL	38/200	0.492	83,445
19	AL	38/200	0.5	89,008

To check whether the proposed set-up had accurate results or not, the results should be compared with the theoretical value that had been calculated using the British standards code for both the steel and the aluminum. For this purpose another excel program were developed to calculate the theoretical value of the moment of inertia. Tables 13 and 14 show the calculated values for the sheet based on the measured dimensions.

Table 13: Steel Sheet Profiles Type and Thicknesses and Their Theoretical Moment

Item	Material type (steel)	Profile	Measured thickness (mm)	Moment of inertia (mm⁴/ m width) (theoretical)
1	GI	32/250	0.634	84,365
2	GI	32/250	0.645	85,877
3	GI	45/150	0.642	239,676
4	GI	45/150	0.652	256,459
5	GI	45/150	0.661	260,892
6	GI	45/250	0.619	132,370
7	GI	45/250	0.622	135,571
8	GI	54/250	0.6235	135,651
9	GI	38/200	0.624	135,791
10	GI	38/200	0.6243	138,300
11	GI	38/200	0.6249	139,355
12	GI	38/200	0.626	136,409
13	GI	38/200	0.635	140,853
14	GI	38/200	0.641	138,439
15	GI	38/200	0.645	144,240
16	GI	38/200	0.648	146,784
17	GI	45/150	0.42	144,101
18	GI	45/150	0.437	147,371
19	GI	45/150	0.4548	158,766
20	GI	38/200	0.71	152,782
21	GI	38/200	0.73	158,990
22	GI	38/200	0.74	155,984
23	GI	38/200	0.4398	90,728
24	GI	38/200	0.4488	93,057
25	GI	38/200	0.455	94,671
26	GI	45/150	0.82	327,034
27	GI	45/150	0.829	330,721
28	GI	45/150	0.835	333,179

Table 14: Aluminum Sheet Profiles Type and Thicknesses and Their Theoretical Moment

Item	Material type (aluminum)	Profile	Measured thickness (mm)	Moment of inertia (mm ⁴ / m width) (theoretical)
1	AL	45/250	0.667	142,811
2	AL	45/250	0.673	152,808
3	AL	32/250	0.69	159,323
4	AL	45/150	0.638	196,139
5	AL	45/150	0.645	194,964
6	AL	45/150	0.648	190,471
7	AL	45/150	0.668	210,925
8	AL	38/200	0.75	145,262
9	AL	38/200	0.75	145,262
10	AL	38/200	0.755	150,450
11	AL	38/200	0.758	155,744
12	AL	38/200	0.773	157,062
13	AL	38/200	0.8456	183,924
14	AL	38/200	0.85	182,078
15	AL	38/200	0.86	186,859
16	AL	38/200	0.885	195,494
17	AL	38/200	0.89	199,429
18	AL	38/200	0.492	80,515
19	AL	38/200	0.5	82,797

Tables 15 and 16 on the following page, show the degree of the accuracy of the proposed machine by finding the difference between the tested value and the theoretical one. The data in Tables 15 and 16 of the proposed set-up shows a small margin of difference between the tested and the calculated one. The difference in steel panels between the tested and the calculated is (1.2%-3.2%) and for the aluminum is (1.7%-3.8%), in both cases the difference is within acceptable limits. This makes the proposed set-up an accurate set-up to simulate the uniform load on the profiled metal sheets. Moreover, after plotting the thickness vs. moment for different profiles, as shown in Figures 45 and 46, it is noticeable that with the increase of the profile thickness the strength increases linearly for the same profile. This means that the thicker the profile the more strength it has, which is expected due to the increase of the moment of inertia.

Table 15: Steel Sheet Profiles Type and Thicknesses and Their Tested & Theoretical Moment

Item	Profile	Measured thickness (mm)	Average thickness	Moment of inertia (mm ⁴ / m width) (Full)	Moment of inertia (mm ⁴ / m width) (theoretical)	Moment of inertia (mm ⁴ / m width) (Tested)	% Error
1	32/250	0.634	0.6395	88,102	85,121	87,941	3.2
2	32/250	0.645					
3	45/150	0.642	0.6517	259,433	252,342	255,620	1.2
4	45/150	0.652					
5	45/150	0.661					
6	45/250	0.62	0.621	183,983	170,533	175,752	3
7	45/250	0.624					
8	45/250	0.619					
9	38/200	0.622	0.6273	153,603	142,244	146,352	2.8
10	38/200	0.6235					
11	38/200	0.622					
12	38/200	0.6243					
13	38/200	0.6249					
14	38/200	0.626					
15	38/200	0.635					
16	38/200	0.641					
17	45/150	0.42	0.4373	172,867	150,079	152,356	1.5
18	45/150	0.437					
19	45/150	0.4548					
20	38/200	0.71	0.7267	178,688	170,939	173,048	1.2
21	38/200	0.73					
22	38/200	0.74					
23	38/200	0.4398	0.4479	108,848	92,819	94,735	2
24	38/200	0.4488					
25	38/200	0.455					
26	45/150	0.82	0.828	331,518	330,311	336,420	1.8
27	45/150	0.829					
28	45/150	0.835					

Table 16: Aluminum Sheet Profiles Type and Thicknesses and Their Tested & Theoretical Moment

Item	Profile	Measured thickness (mm)	Average thickness	Moment of inertia (mm ⁴ /m width) (Full)	Moment of inertia mm ⁴ / m width) (theoretical)	Moment of inertia (mm ⁴ / m width) (Tested)	% Error
1	45/250	0.667	0.67	198,839	145,810	149,800	2.6
2	45/250	0.673					
3	32/250	0.69	0.69	95,307	77,870	80,547	3.3
4	45/150	0.638	0.6498	258,661	198,125	202,644	2.2
5	45/150	0.645					
6	45/150	0.648					
7	45/150	0.668					
8	38/200	0.75	0.757	186,376	150,756	153,455	1.7
9	38/200	0.75					
10	38/200	0.755					
11	38/200	0.758					
12	38/200	0.773					
13	38/200	0.8456	0.866	214,190	187,341	190,960	1.9
14	38/200	0.85					
15	38/200	0.86					
16	38/200	0.885					
17	38/200	0.89					
18	38/200	0.492	0.496	120,782	73,589	76,524	3.8
19	38/200	0.5					

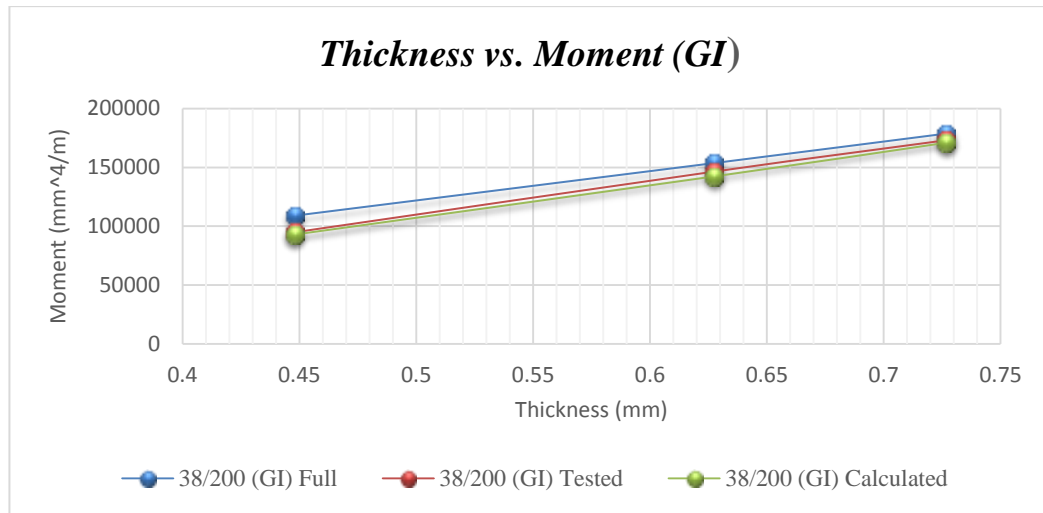


Figure 47: Moment of Inertia vs. Thickness for (GI 38/200) Profile with Different Thicknesses

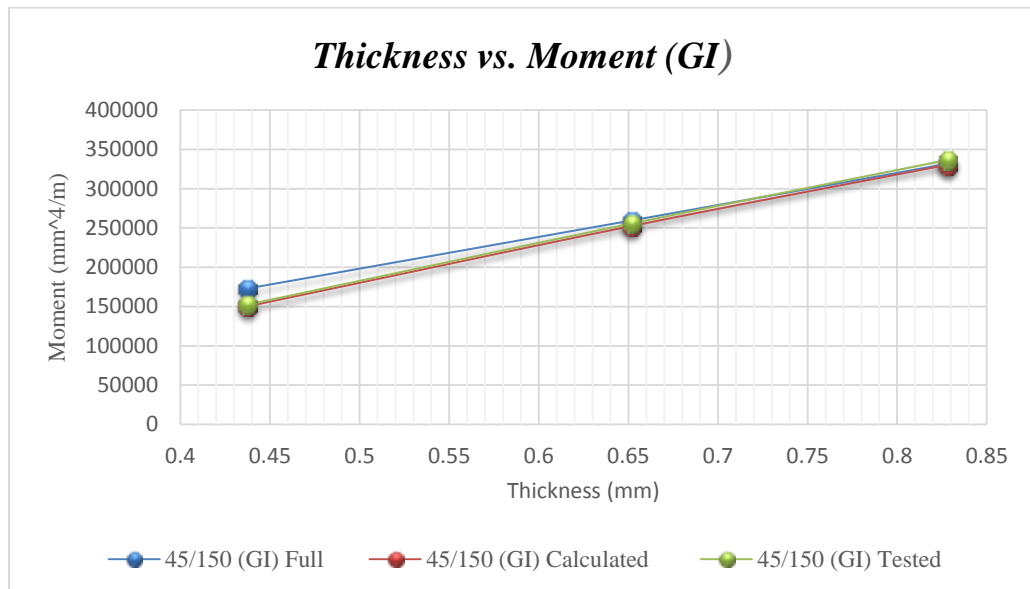


Figure 48: Moment of Inertia vs. Thickness for Different Profile with Different Thicknesses

Furthermore, the full moment before loading for any profile made of any metal is the same and it starts to reduce after loading, as shown in Tables 15 and 16 above. However, the reduction is different from one metal to the other. The moment reduction is lower in the steel than aluminum, as shown on Figures 49 and 50. Moreover, the thicker and stiffer the profile the less reduction in the moment of the profile. The reason behind that is due to the effect of the local buckling, which is reduced in the profile. This is shown in Figures 48 and 49.

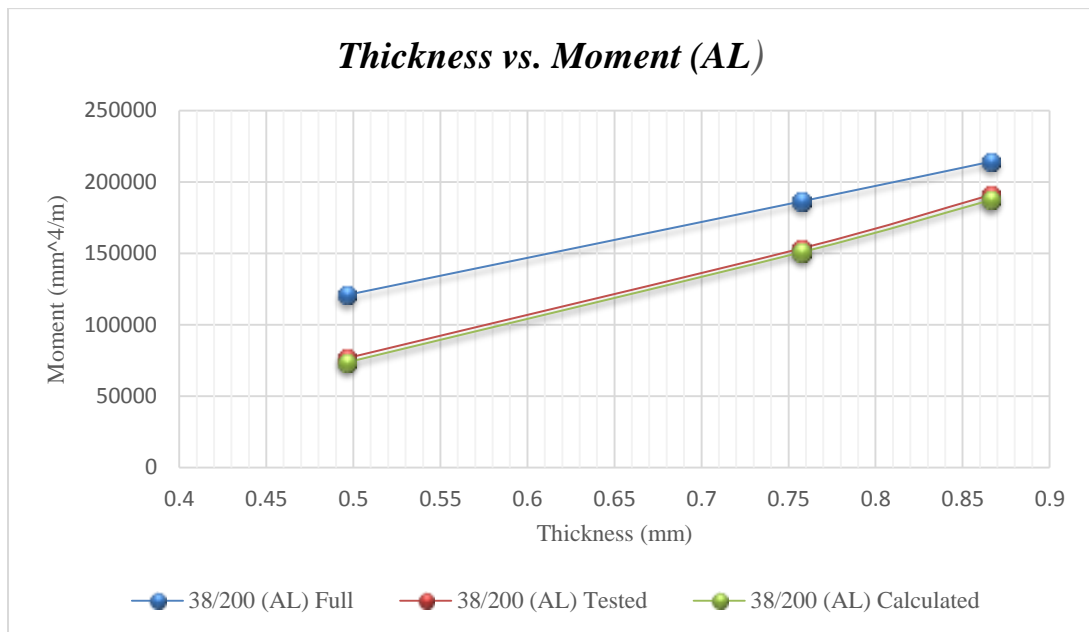


Figure 49: Moment of Inertia vs. Thickness for (AL 38/200) Profile with Different Thicknesses

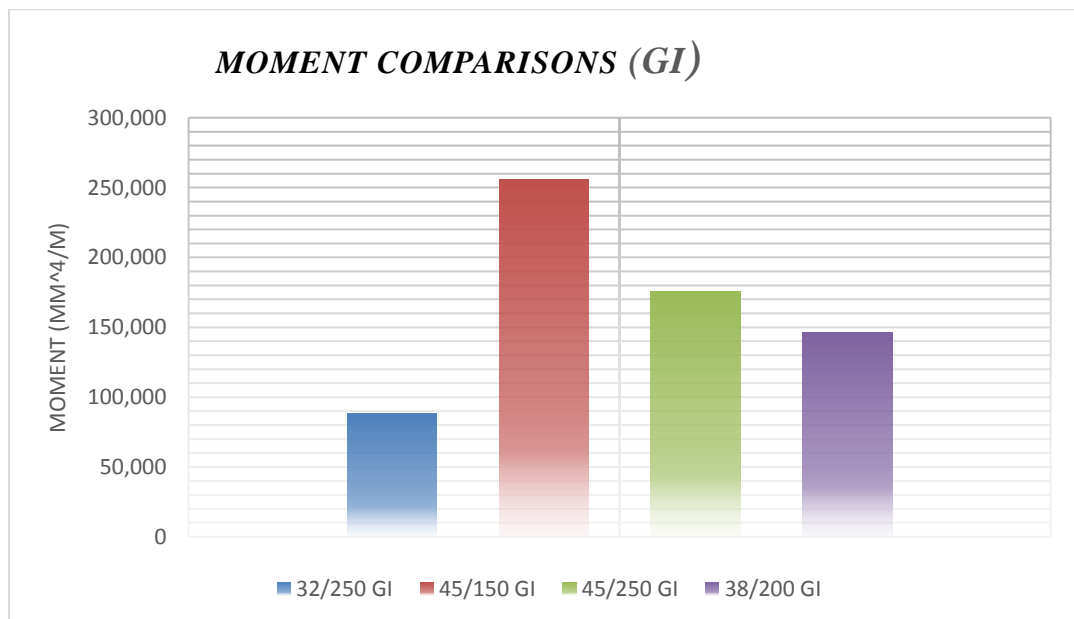


Figure 50: Moment of Inertia Capacity for Different Profiles with the Same Thickness (0.7mm)

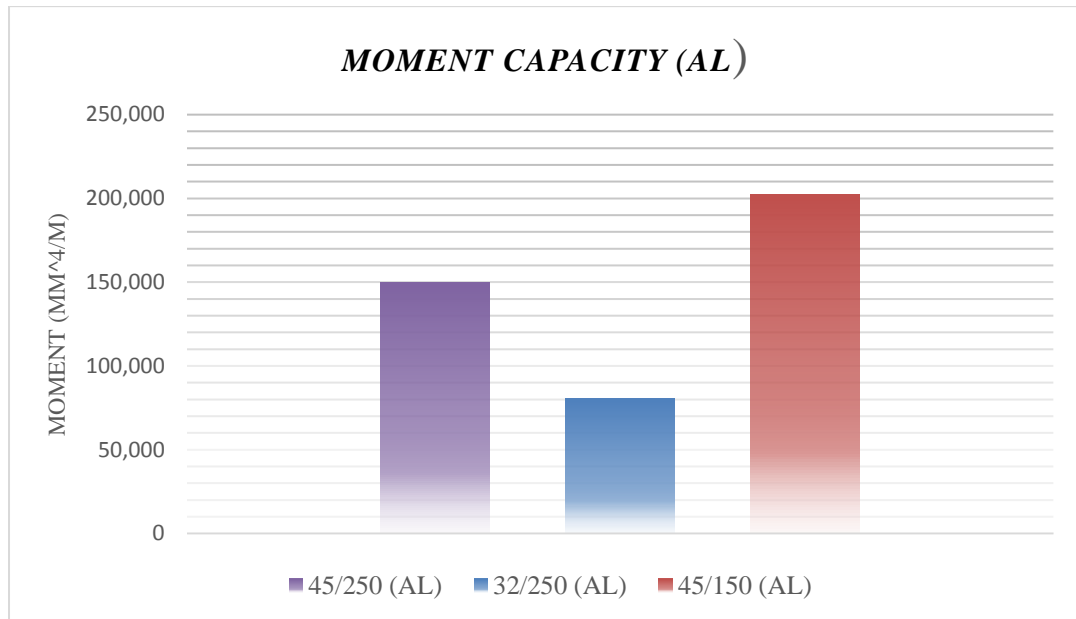


Figure 51: Moment of Inertia Capacity for Different Profiles with the Same Thickness (0.7 mm)

Another important observation is that the higher the profile and the less distance between them the higher the strength of the profile. The reason behind that is the profile becomes stiffer. Figures 51 and 52 show the moment for different profiles with the same thickness. It is clear that the profile (45/150) has the biggest moment which means this is the strongest between profiles for both the steel and aluminum. Nevertheless, even though the profile (45/150) is the strongest, it covers less surface area than other profiles which makes it more expensive than other profiles. The selection of the profile type and thickness depends on the application of the profile which provides optimum cost.

Moreover, the metal type of the profile plays a role in the strength of the profile. As it was mentioned before the full moment of all profile is the same. However, it changes after loading and, as it is clear in Figure 53 the aluminum lost more of its moment during loading than steel for the same profile with the same thickness. The reason behind that is that aluminum is generally half as strong as steel, but much lighter, which makes more reduction in the moment.

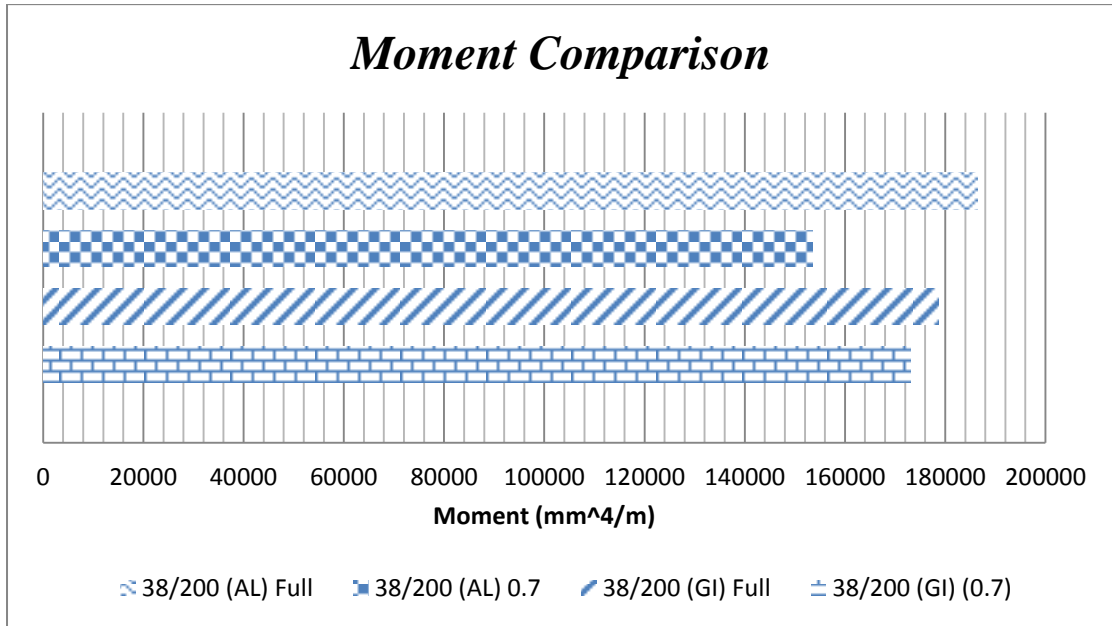


Figure 52: Moment Comparison between Steel Profiles and Aluminum Profiles with the Same Thickness

Analysis Using ABACUS

The values obtained using FE Model (Figure 54) were based on the load required to make the steel sheet deflects to the limits $L/90$. Those values are shown in Table 17. Moreover, from those loads and the constant deflection value, the value of the moment of inertia was obtained and compared with the tested value and the calculated value. The load was applied as pressure (N/mm). The calculated deflection range was obtained from the code:

$$\frac{L}{90} = \frac{2000mm}{90} = 22.22mm$$

The moment of inertia for the FE model is calculated using the equation below:

$$\Delta = \frac{(5 * pL^4)}{385EI}$$

$$I = \frac{385E\Delta}{(5 * pL^4)}$$

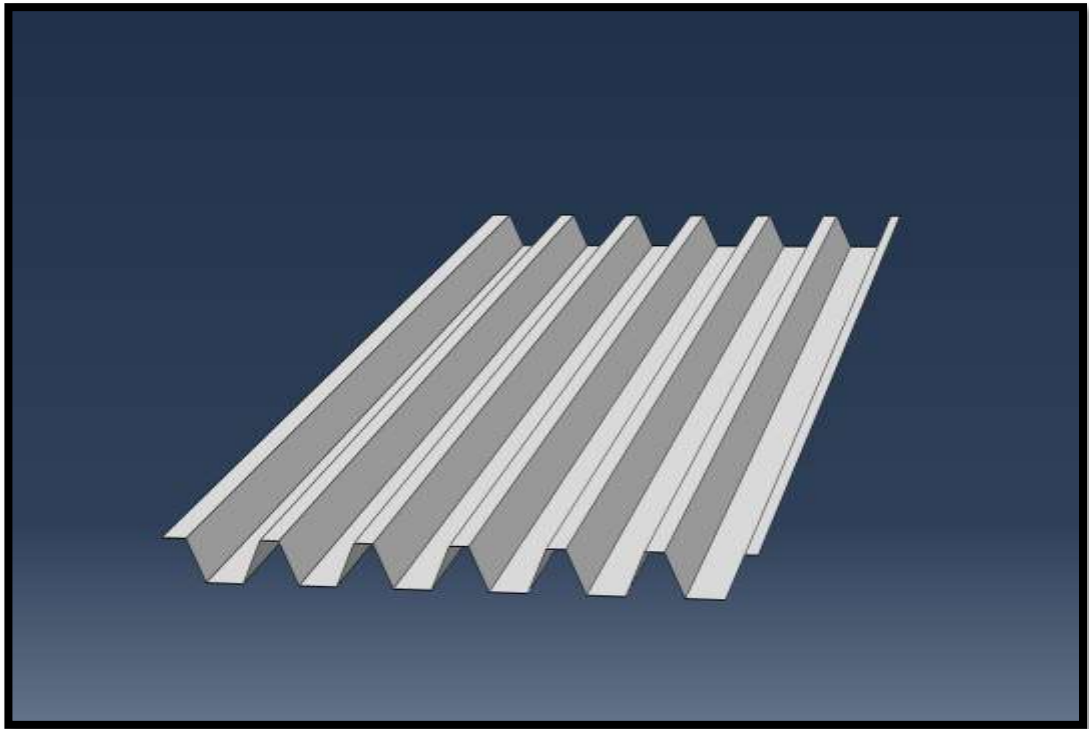


Figure 53: FE Model

Table 17: (38/200) Profiled Steel Sheet Load and Moment Using Finite Element Model

Measured thickness (mm)	Load (N)	Deflection (mm)	FE(mm ⁴ / m width)
0.619	12.38389	22.22	139,863
0.622	12.44644	22.22	140,705
0.6235	12.49145	22.22	141,140
0.624	12.51125	22.22	141,285
0.6243	12.5225	22.22	141,372
0.6249	12.53825	22.22	141,546
0.626	12.56526	22.22	141,866
0.635	12.80378	22.22	144,487
0.641	12.9613	22.22	146,243
0.645	13.06031	22.22	147,416
0.648	13.16382	22.22	148,297

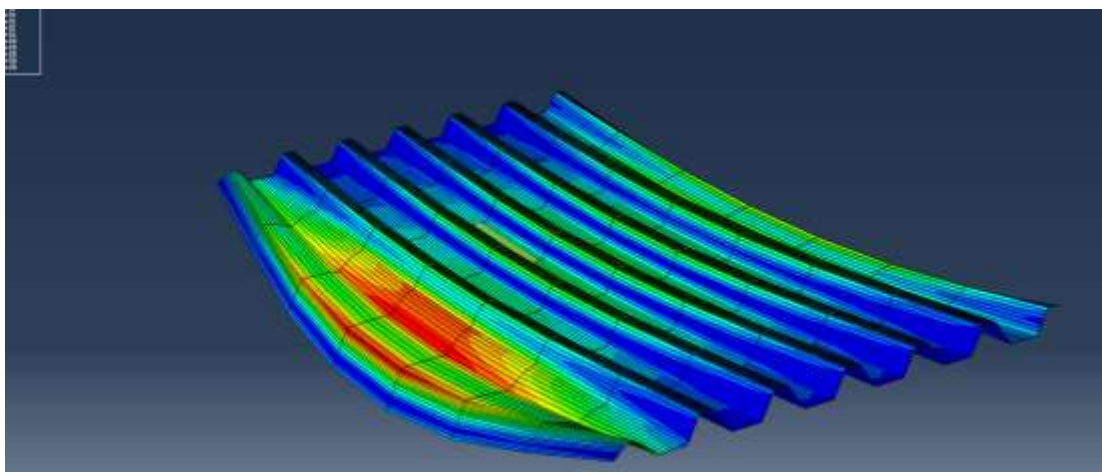
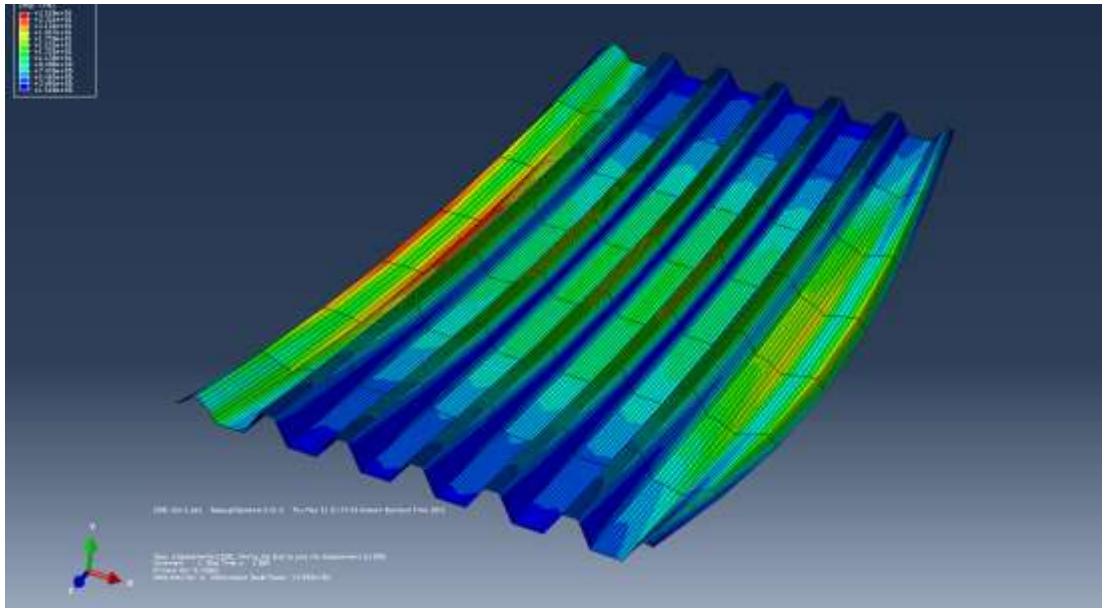


Figure 54: Deflected FE Model

Figures 56 and 57 show the comparison between the FE model and the tested and the calculated values of 38/200 steel profile.

As it is clear in the graph, the model has given a constant increase rate. The moment of inertia was constantly increased with thickness which is normal. However, in the model the manufacturing variation in the dimensions and material defects were not considered due to those consideration a linear increase can be seen in the graph. Furthermore, the model value was higher from both the tested and the calculated values of the moment of inertia, the reason for this difference is that the model does not take into account the reduction factors for the capacity of the profile, plus it assumes a perfect conditions in the model when in reality it is impossible to obtain

perfect conditions. There are always an installation errors, this is why the model has a higher value the tested one.

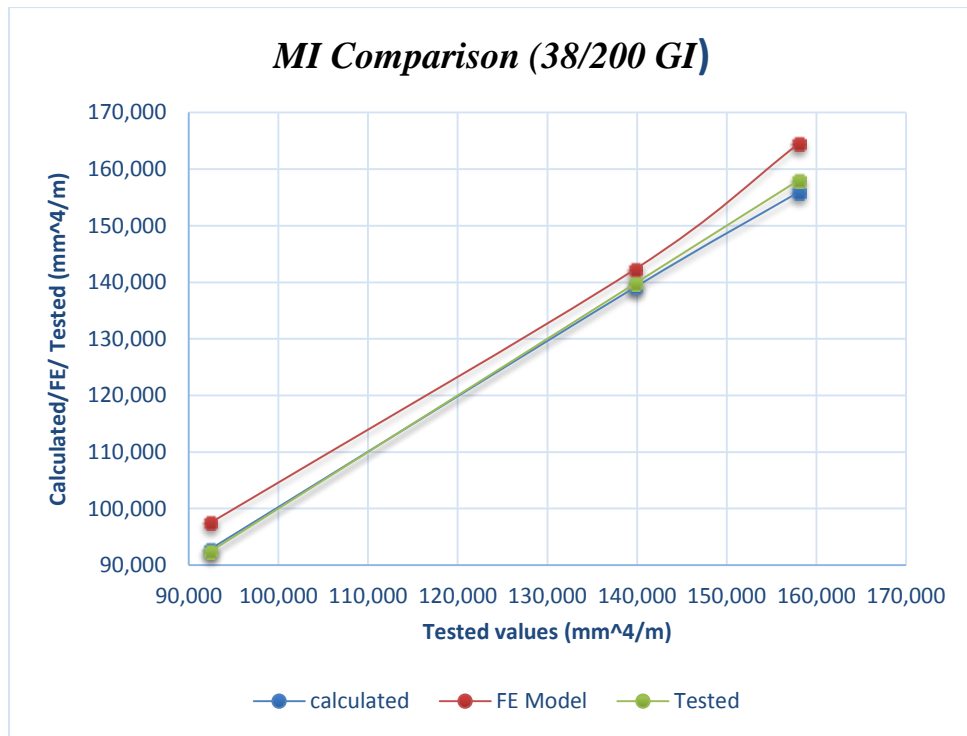


Figure 55: Moment Comparison

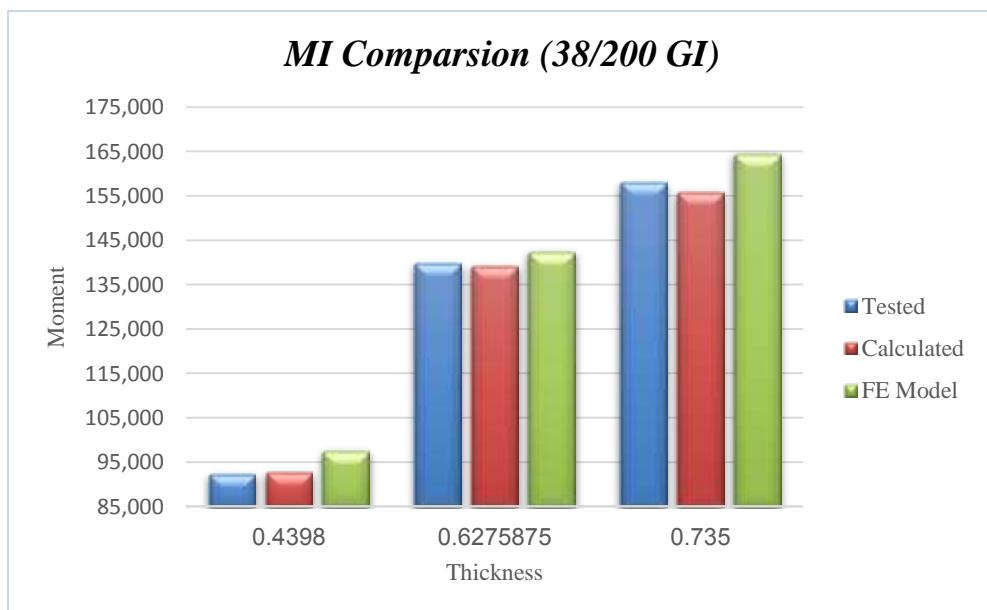


Figure 56: MI comparison For (38/200) Steel Profile with Different Thicknesses

Chapter 6: Conclusions

The use of profiled metal sheets has spread all over the world due to their wide applications in many fields. There exists few testing methodologies to evaluate their mechanical characteristics, specifically their moment of inertia. These methodologies are complicated and time consuming. In this study, a new testing set up as well as testing procedures were developed to measure the effective moment of inertia of profiled sheets. Both galvanized steel and aluminum can be performed in an easy manner that provides for accurate measurements.

The following conclusions can be drawn from this study:

1. Profiling of metal sheets can increase their strength significantly, making them structural elements.
2. The moment of inertia of the profiled metal sheets depends on the shape of the profile. The higher the profiles and less distance between them the stronger they become.
3. The type of the metal used in the sheets affects the strength of the profile. The stronger the metal the stronger the profile (less local buckling effect). In this study only steel and aluminum were used, and it was found that steel has stronger profiles for the same parameter (profile shape and thickness).
4. The thicker the profile the less reduction in the full moment of the profile, which produces a stiffer and stronger profile (less local buckling effect).
5. The difference between the actual tested samples and the empirical calculations for the galvanized steel profiles are 1.2%-3.2%. The results mean the new set up produced more conservative measurements compared to the empirical calculations. This is due to the safety factor imbedded within the empirical equations.
6. Similarly, the aluminum profiled shows the same pattern which is 1.7%-3.8% due to the same reason above.
7. Furthermore, modeling by ABACUS has shown close differences from the tested values which supports the current results.

Moreover, a theoretical calculation based on the British Code was applied to check the accuracy of the tested values. Similarly, an FE model was developed to compare the perfect conditions with the tested and observed change in values. In the end, all the values from the testing, calculations and modeling were compared and it was found that the values for the tested panels were below the model values (perfect conditions) and higher than the calculated values. The set-up produced an approximate value for the metal sheet, which makes it suitable for testing in manufacturing factories or at sites.

References

- [1] American Iron and Steel Institute (AISI), “Specification for Design of Cold Formed Steel Structural Members.” AISI, Washington, DC, 1996.
- [2] Cook, N. J. “The Designer Guide to Wind Loading of Buildings and Structures.” *Building Research Establishment Report*, vol. 2, pp. 87-92, 1990.
- [3] Y.L. Xu, “Behavior of Different Profiled Roofing Sheets Subjected to Simulated Wind Uplifting.” Technical Report no. 37, Cyclone Testing Station, James Cook University, Australia, 1994.
- [4] BlogSpot. “Metal Roof.” *Blogspot.ae*. [Online]. Available <http://metalrooftoday.blogspot.ae/2011/12/use-clean-metal-roof.html> [Accessed: May 10, 2015].
- [5] D. Prevatt and S. Schiff, “Uplift Testing of Standing Seam Metal Roof Systems.” Research Report, Clemson University MBMA Project 903, South Carolina, 1996.
- [6] J. Malpezzi and R. Gillenwater, “Static vs. Dynamic: A Wind Uplift Testing Study,” presented at the 10th Conference on Roofing Technology, Gainesville, Florida, 1993.
- [7] G. Winter, “Commentary on the Specification for the Design of Cold-Formed Steel Structural Members.” American Iron and Steel Institute, Washington, DC, 1970.
- [8] Ho, T. C. E., and D. Surry, “Factory Mutual—High-Resolution Pressure Measurements on Roof Panels.” The University of Western Ontario, Boundary Layer Wind Tunnel Laboratory Report: BLWT – SS11- 2000, 2004.
- [9] S. Hensen, “Open Front Structure Wind Pressure Design.” February 23 2013. [Blog entry]. *Structural Engineering Blog*. Available <http://seblog.strongtie.com/2013/02/open-front-structure-wind-pressure-design> [Accessed: September 15 2015]

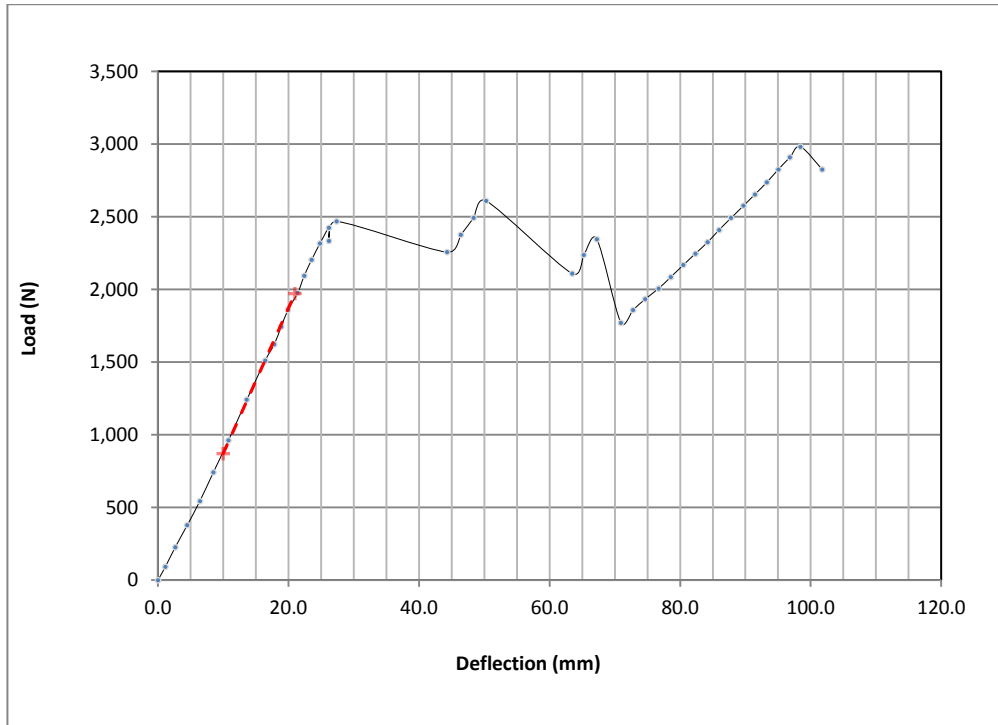
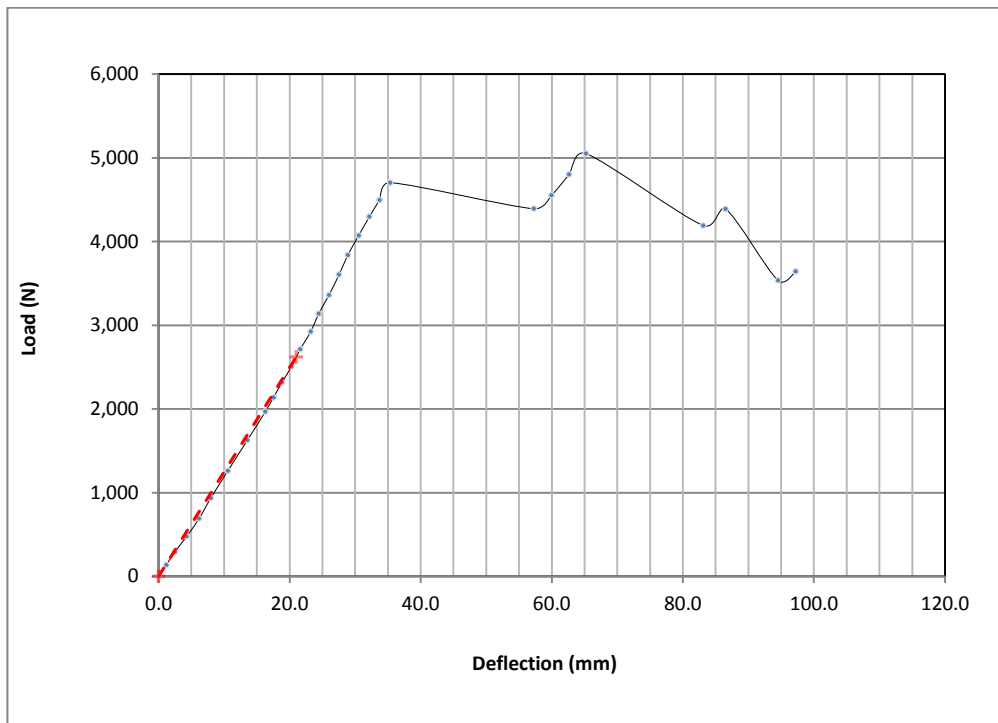
- [10] C. Yu, “Distortional Buckling of Cold-Formed Steel Members in Bending.” Ph.D. Thesis, Johns Hopkins University, Baltimore, MD, 2005.
- [11] V.R. Beck and L.K. Stevens, “Wind Loading Failures of Corrugated Roof Cladding,” presented at the Diamond Jubilee Conference, Institution of Engineers, Perth, Australia, 1979.
- [12] ASTM E1592-05, “Standard Test Method for Structural Performance of Sheet Metal Roof and Siding Systems by Uniform Static Air Pressure Difference.” ASTM International, West Conshohocken, PA, 2012.
- [13] D. Surry, et al., “Structurally Effective Static Wind Loads for Roof Panels.” *Journal of Structural Engineering*, ASCE, pp. 871-885, June 2007.
- [14] M.J. D’Costa and F.M. Bartlett, “Full-Scale Testing Of Corrugated Fibreboard Shelter Subjected To Static-Equivalent Wind Loads.” *Journal of Wind Engineering and Industrial Aerodynamics*, 91 (12-15), pp. 1671-1688, 2003.
- [15] D. Mahaarachchi and M. Mahendran, “Finite Element Analysis and Design of Crest-fixed Trapezoidal Steel Claddings with Wide Pans Subject to Pull-through Failures.” *Engineering Structures*, 26 (11): 1547-1559, p. 154, 2004.
- [16] D. Henderson, J. Ginger, M. Morrison, and G.A. Kopp, “Simulated Cyclonic Winds for Low Cycle Fatigue Loading Of Roofing.” *Wind and Structures*, vol. 12, pp. 383-400, 2009.
- [17] R.R. Sinno, “Simulation of Uplift Loading on Thin Metal Roofs (Electromagnetic Uplift Testing).” MBMA Final Report, Dec. 2005.
- [18] B. Abbas, H. Faleh, and A. Al-Tamimi, “*Structural Performance Of Polyurethane Injected Sandwich Panels under Flexural Loads*,” presented at the IMS/6 International Conference of Materials Applications, Sharjah, UAE, 2012.
- [19] British Standards Institution, “Eurocode 3: Design of Steel Structures: Part 1.3: General Rules—Supplementary Rules for Cold-Formed Thin Gauge Members and Sheeting.” London, UK, BS EN, 1993-1-3, 2006.

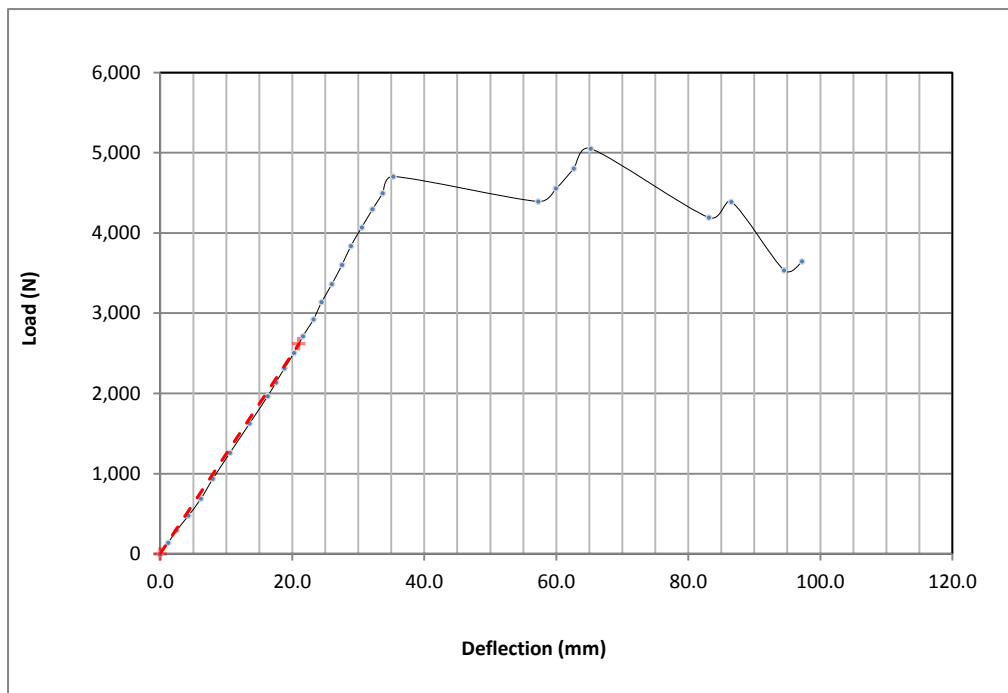
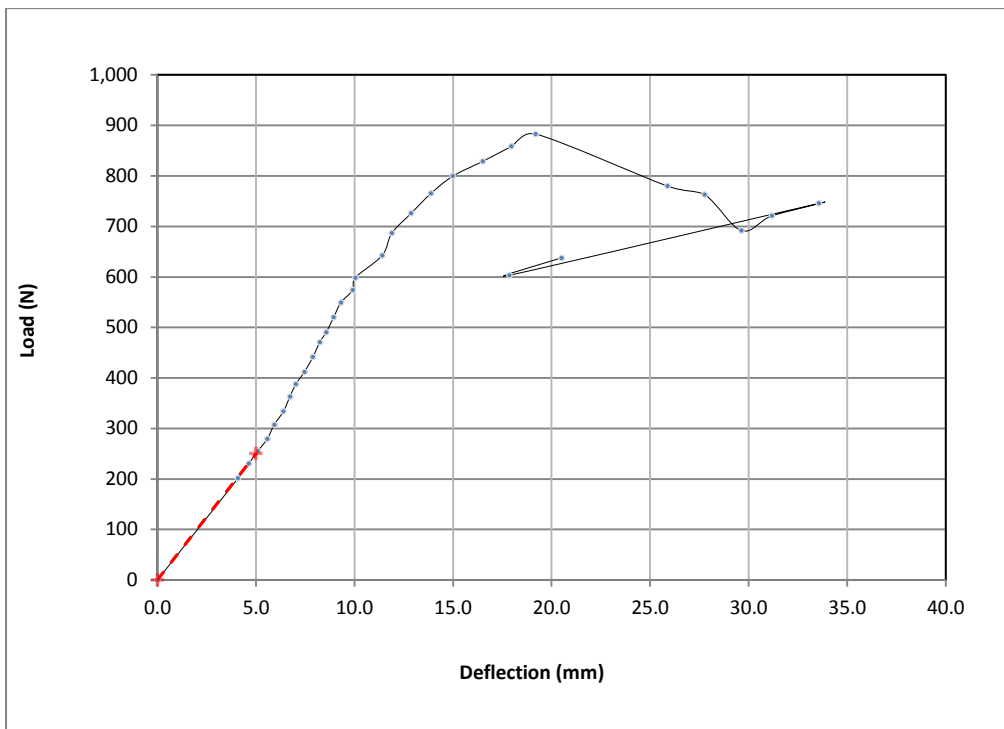
- [20] European Committee for Standardization, “Eurocode 9: Design of Aluminum Structures - Part 1-4: Cold Formed Structural Sheeting.” EN, 1999-1-4/A1, 2007.
- [21] “Profiled Metal Roofing Design Guide.” Technical Report no. 6, The Metal Cladding & Roofing Manufacturers Association Limited, Cheshire, UK, June 2004.
- [22] M. Mahendran, “Fatigue Behavior of Corrugated Roofing under Cyclic Wind Loading.” Technical Report no. 35, Cyclone Testing Station, James Cook University, Australia, 1990.
- [23] M. Mahendran, “Static Behavior of Corrugated Roofing under Simulated Wind Loading.” Technical Report no. 33, Cyclone Testing Station, James Cook University, Australia, 1990.
- [24] G.A. Kopp, Y. Chen, and D. Surry, “Wind Effects on Rooftop Elements on Low Buildings: Phase 1. Basic Factors Governing Loads.” Wind Engineering Group Report no. BLWT-SS40-2003, University of Western Ontario, London, Canada, 2003.
- [25] R.R. Sinno, D. Surry, S. Fowler, and T.C.E. Ho, “Testing of Metal Roofing Systems under Realistic Wind Loads,” presented at the 11th International Conference of Wind Engineering, Texas Tech University, Lubbock, Texas, 2003.
- [26] American Institute of Steel Construction, “Specification for Structural Steel Buildings — Allowable Stress Design and Plastic Design,” Chicago, IL, 1989.
- [27] American Iron and Steel Institute Standard S100 Supplement no. 2, “North American Specification for the Design of Cold-Formed Steel Structural Members,” Washington, DC, 2007.
- [28] N.J. Cook, A.P. Keevil, and R.K. Stobart, “BRERWULF- The Big Bad Wolf.” *Journal of Wind Engineering and Industrial Aerodynamics*, vol. 29, pp. 99-107, 1980.

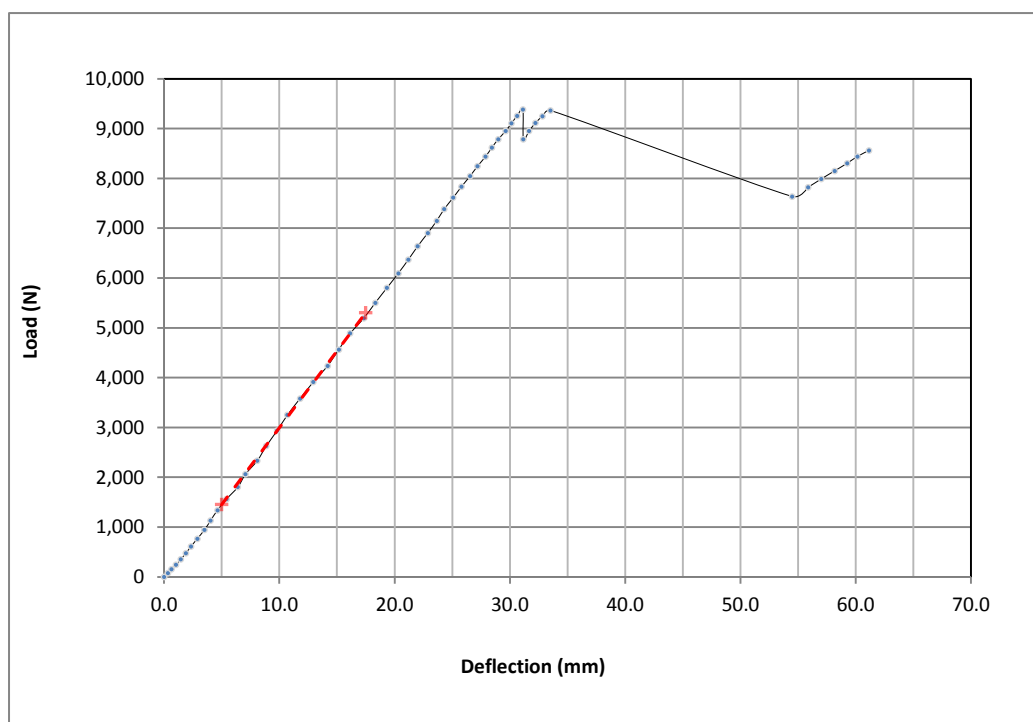
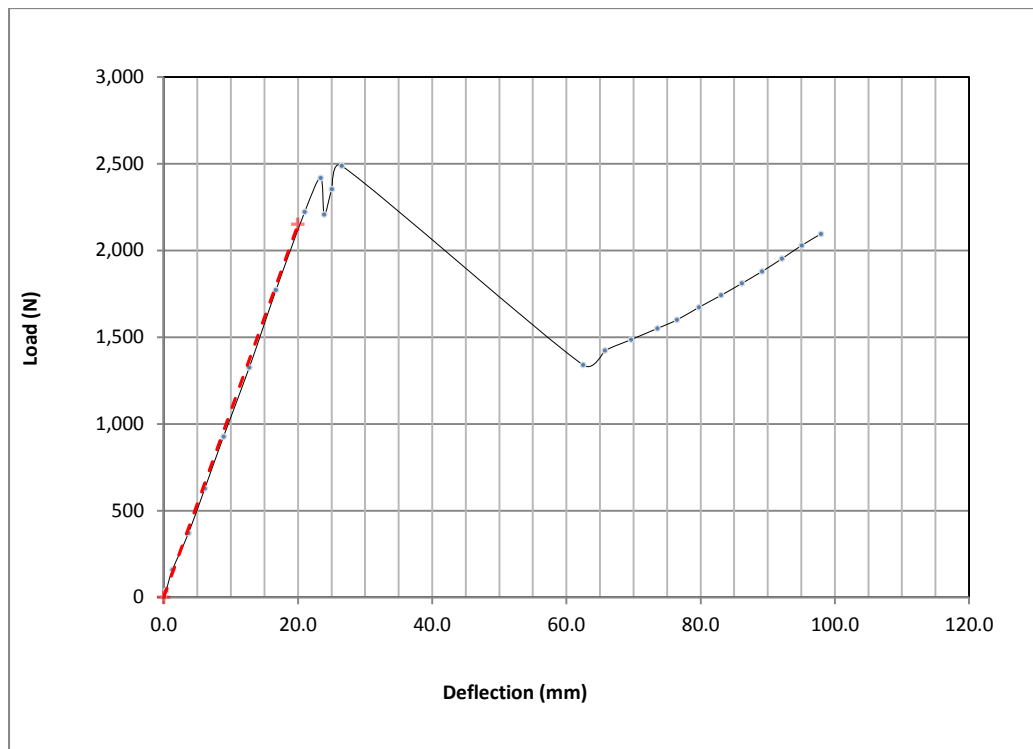
- [29] S. Farquhar, G.A. Kopp, and D. Surry, “Wind Tunnel and Uniform Pressure Testing Of A Standing Seam Metal Roof Model.” *Journal of Structural Engineering*, vol. 131, pp. 272-279, 2003.

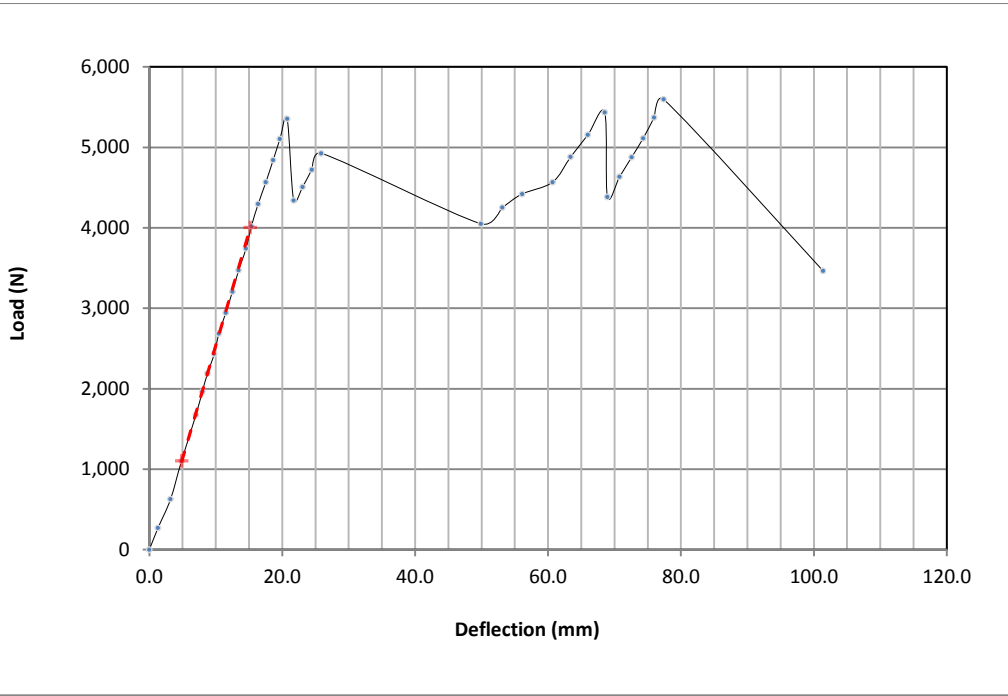
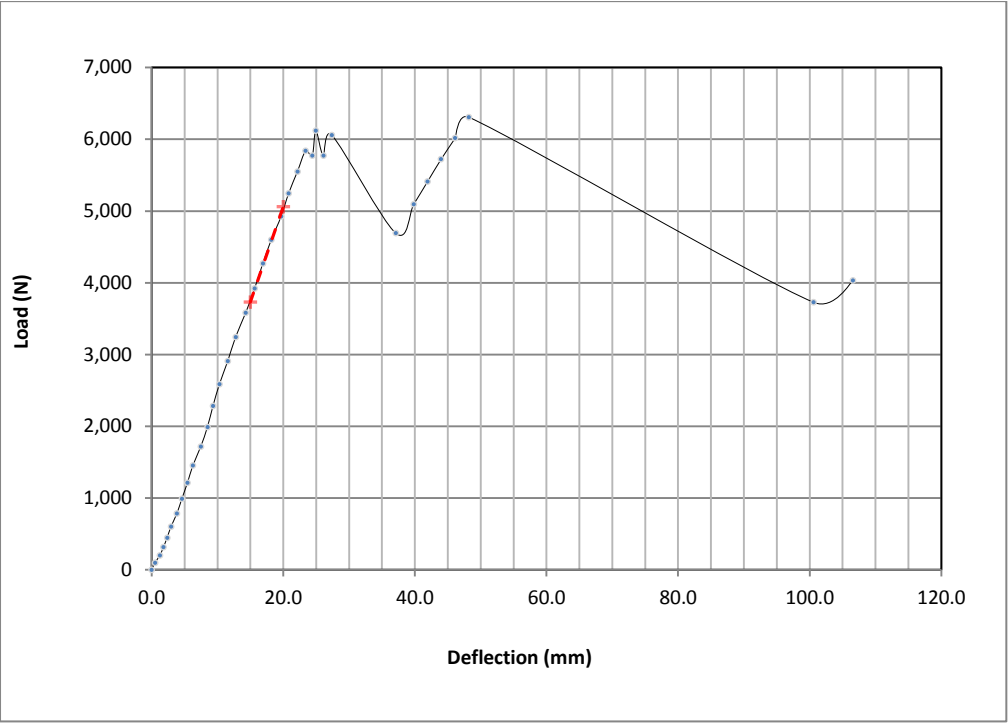
Appendix

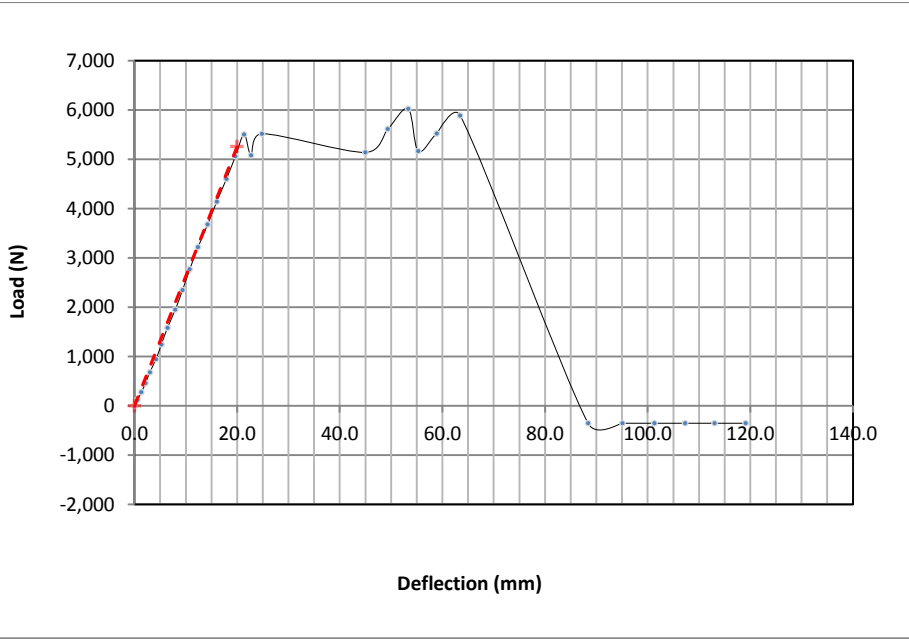
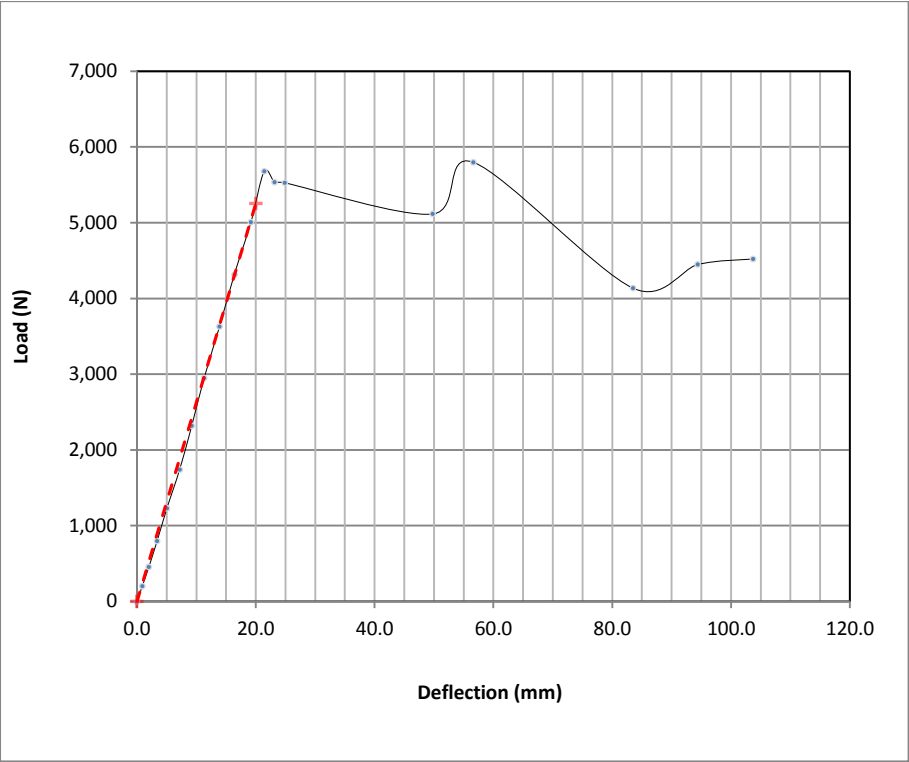
Load - Deflection Graphs for Various Profiled Sheets

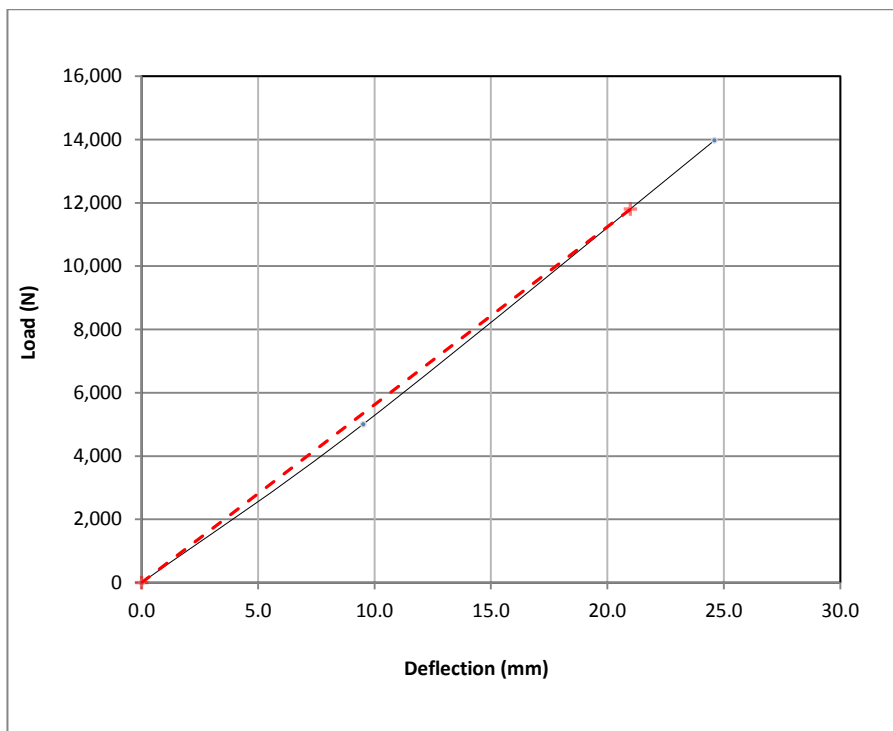
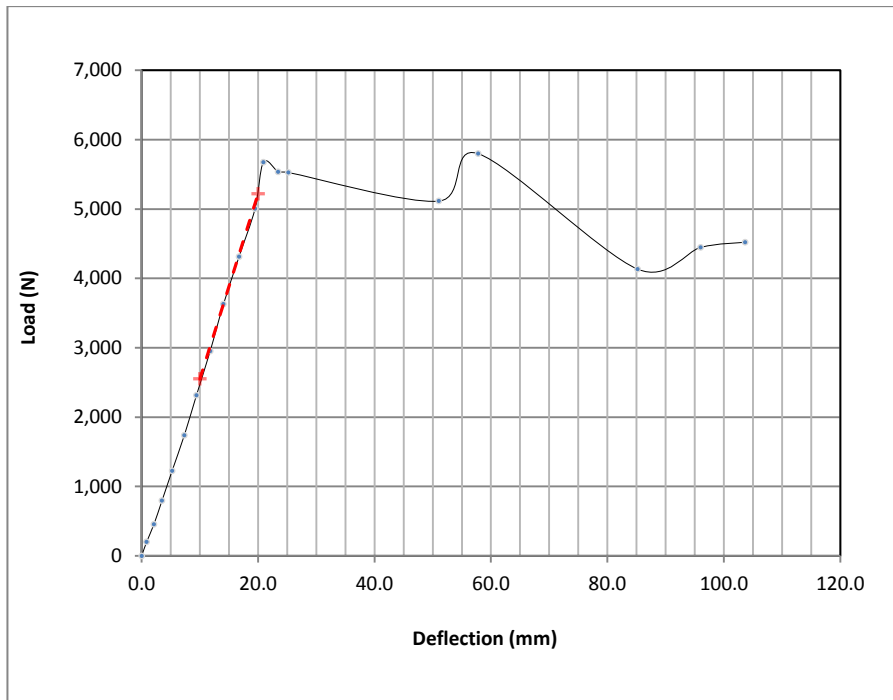












Vita

Hassan Al Qaraghuli was born in Nasriya, on May 5th 1990 in Iraq. He was educated in both public and private schools across Iraq, Syria and the United Arab Emirates (UAE). He graduated from New World High School in 2008 with honors from the UAE. He received a scholarship to attend the American University of Sharjah where he graduated with a Bachelor's in Civil Engineering and a minor in Environmental Engineering.

Mr. Qaraghuli has been the manager of Al Tawauun Feed Mill since 2013. In the same year he pursued his Master's degree in Civil Engineering at the American University of Sharjah.

Mr. Qaraghuli is currently a member of the Iraqi Businessman Union based in Iraq.